



**Politecnico
di Torino**

**Master's Degree in Environmental Engineering
Natural Hazards and Civil Protection**

Master's Degree Thesis

**Design of new types of rockfall barriers:
from sensitivity analysis to machine
learning**

Supervisors:

Prof. Vagnon Federico

Candidate:

Labbrozzi Federica

CoSupervisors:

Prof. Depina Ivan

Prof. Migliazza Maria Rita

Eng. Carriero MariaTeresa

March 2025

*A me,
alla mia famiglia,
alle mie sorelline e fratellini fedeli.*

Abstract

Landslides, especially rockfalls, present a major threat to the safety of infrastructure and communities, making it crucial to develop effective protective measures. Hybrid rockfall barriers, known as attenuators, present an intriguing option in this context as they merge the capacity to absorb impact energy with the regulation of block trajectories. However, many factors, such as geomorphological, topographical and vegetation characteristics, as well as dynamic effects, such as dynamic response of the net and stress distribution at the block impact, influence the design of such systems, making it complex. In order to simplify and generalize the design parameters, this thesis aims to identify the most important parameters for attenuators analysis. The block volume, velocity and direction of impact were selected through a literature review. Subsequently, combining these variables, a parametric analysis was conducted using Abaqus/CAE software. The results showed that some parameters have a greater impact than others, suggesting the need for a more sophisticated method to find correlations. For this reason, a machine learning algorithm was used, which enabled a global parametric analysis to be performed. In particular, the algorithm includes detecting correlations between parameters using Pearson's coefficient and studying interactions at the moment of impact. By using the results extrapolated from Abaqus/CAE, the output values of the simulations were modelled with a deep learning model based on LSTM networks. In this context, incorporating artificial intelligence represents a significant innovation as it enhances predictive abilities and streamlines design processes, decreasing the number of necessary simulations and yielding more dependable outcomes. This ultimately facilitates the creation of more effective guidelines for rockfall protection. Additional research efforts could focus on improving the machine learning algorithm and expanding the dataset with more complex simulations and experimental verifications, to further enhance the reliability of predictive models.

Table of Contents

List of Tables	IV
List of Figures	V
Acronyms	IX
1 Introduction	1
1.1 Background and motivations	1
1.2 Objectives	2
1.3 Limitations	3
2 Rockfall phenomena	5
2.1 Landslide phenomena	5
2.2 Rockfall phenomena	9
2.3 Rockfall protection structures	10
2.4 New types of protection structures	11
2.4.1 Essential elements of innovative rockfall barriers	13
2.4.2 Hybrid barrier and attenuator design	17
2.5 Rockfall barriers legislation	19
2.5.1 European Normative	20
2.5.2 Current and future design methods	21
3 Numerical Modelling in Abaqus/CAE	23
3.1 Software introduction	23
3.2 Model geometry	24
4 Sensitivity analysis	28
4.1 Selection of input parameters	29
4.2 Local sensitivity analysis	29
4.2.1 Volume	35
4.2.2 Traslational velocity	38

4.2.3	Rotational velocity	41
4.2.4	Impact angle	44
4.2.5	Impact position along Y	47
4.2.6	Impact position along Z	50
5	Machine learning	53
5.1	Machine learning	55
5.1.1	How it works - ML	56
5.2	Artificial neural networks	57
5.2.1	How it works - ANN	58
5.2.2	Feedforward vs. Recurrent Neural Networks	60
5.2.3	Benefits of ANNs	61
5.3	Global sensitivity analysis	61
5.3.1	Input Parameter Selection	62
5.3.2	Machine Learning Dataset Creation	63
5.3.3	Machine Learning Deployment	65
6	Epilogue	81
6.1	Conclusion	81
6.2	Suggestion	82
	Bibliography	84

List of Tables

4.1	Basic set up for parametric analysis	29
4.2	Slope and net characteristics	30

List of Figures

2.1	Landslide classification	6
2.2	Landslide classification - movement rate	7
2.3	Population at landslide risk	7
2.4	Percentage landslide index	8
2.5	Example of rockfall event	9
2.6	Rockfall mechanism	10
2.7	Rockfall protection barriers	12
2.8	View of prototype attenuator system installed in Stanwell Park by Geobrugg [13] [GeoBrugg]	13
2.9	Attenuator main zone [14]	14
2.10	Model to be implemented	15
2.11	Net fence detail	16
2.12	Net fence detail: posts	16
2.13	Net fence detail: dissipation element	17
3.1	Flowchart Example	23
3.2	Implemented flowchart	24
3.3	Geometry of ground surface	25
3.4	rockfall barriers	25
3.5	rock block geometry	26
3.6	Module <i>Assembly</i> of the structure	27
4.1	Variation of chosen parameters	30
4.2	Schematic definition of a_{max} [Courtesy of Carriero MariaTeresa from her PhD thesis (in submission)]	31
4.3	Abaqus representation of interception net, view from above	31
4.4	Analysis diagram for the upper cable [Courtesy of Carriero Mari- aTeresa from her PhD thesis (in submission)]	32
4.5	Diagram of the portion of the sphere in contact with the barrier during impact [Courtesy of Carriero Maria Teresa from her PhD thesis (in submission)]	32

4.6	Scheme for α representation [Courtesy of Carriero Maria Teresa from her PhD thesis (in submission)]	33
4.7	Block acceleration VS Upper cable deformation	33
4.8	Block acceleration VS Kinetic energy during time	34
4.9	Net stresses during time	34
4.10	Relation between Impact acceleration and Volume of the block	35
4.11	Relation between Deformation of the upper cable and Volume of the block	36
4.12	Relation between Energy variation during the impact and volume of the block	36
4.13	Relation between stresses on the cables and the volume of the block	37
4.14	Relation between Impact acceleration and traslational velocity of the block	39
4.15	Relation between deformation of the upper cable and traslational velocity of the block	40
4.16	Relation between Energy variation during the impact and rotational velocity of the block	41
4.17	Relation between Impact acceleration and rotational velocity of the block	42
4.18	Relation between deformation of the upper cable and rotational velocity of the block	43
4.19	Relation between Energy variation during the impact and rotational velocity of the block	44
4.20	Structure diagram with reference system considered [Courtesy of Carriero MariaTeresa from her PhD thesis (in submission)]	45
4.21	Relation between Impact acceleration and impact angle of the block	46
4.22	Relation between deformation of the upper cable and impact angle of the block	46
4.23	Relation between Energy variation during the impact and impact angle of the block	47
4.24	Relation between Impact acceleration and impact position along Y axis	48
4.25	Relation between deformation of the upper cable and impact position along Y axis	49
4.26	Relation between Energy variation during the impact and impact position along Y axis	49
4.27	Relation between Impact acceleration and impact position along Z axis	50
4.28	Relation between deformation of the upper cable and impact position along Z axis	51

4.29	Relation between Energy variation during the impact and impact position along Z axis	51
4.30	Influential parameters chosen for subsequent analysis	52
5.1	Machine learning applications [Bluewind]	53
5.2	Relationship between AI, ML, Neural networks and DL [Machine Learning]	54
5.3	Different types of machine learning algorithm [25]	55
5.4	Similarity between neurons in the human body and neural networks [Dreams]	58
5.5	Multilayered artificial neural network [CNN]	59
5.6	How recurrent neural network works [Deep learning]	60
5.7	Input parameter combinations: local analysis (left) and global analysis (right).	63
5.8	Python scripts used to create the machine learning dataset.	64
5.9	Flowchart of machine learning algorithm	66
5.10	Correlation between input parameters.	67
5.11	Correlation between input parameters and outputs at impact time	68
5.12	Correlation between output parameters at time of the impact	69
5.13	Correlation between inputs and outputs after impact time	70
5.14	Correlation between outputs after impact time	71
5.15	Traslational velocity extrapolated by Abaqus simulation	75
5.16	Velocity trend considering polynomial regression	76
5.17	Velocity trend training the model only on speed values	77
5.18	Combinations of simulated velocity extrapolated	78
5.19	Combinations of calculated velocity extrapolated	78
5.20	Simulated velocity without physical correction	78
5.21	Calculated velocity without physical correction	79
5.22	QR code redirecting to the code's folder [link: GitHub]	80

Acronyms

AI

artificial intelligence

ML

Machine learning

DL

Deep learning

bs

Batch size

Chapter 1

Introduction

1.1 Background and motivations

The phenomenon of rockfalls is widespread both in Italy and worldwide, especially in hilly and mountainous areas. It involves the detachment of blocks of rock of varying size that can fall down the slope following different trajectories. Preventing and mitigating these events is crucial to minimizing damage in populated areas and in locations with critical infrastructure.

Although the phenomenon cannot always be predicted with certainty, investigations can still be carried out to understand the susceptibility of the slope to fracturing, through, for example, hazard analyses. The definition of the hazard of the phenomenon takes place on the basis of the invasion area, the probability of occurrence and the energy involved. In addition to the hazard, the definition of the vulnerability and the value of the exposed elements are also necessary to study the degree of risk.

Thanks to this analysis, a general view of the hazard affecting the studied zone can be obtained and the need to introduce protective structures can be derived.

As will be illustrated in the thesis, structures that provide protection against rockfalls come in various type; Traditional mitigation techniques, such as rigid barriers and embankments, have long been used to address rockfall hazards. However, recent advancements have led to the development of hybrid barriers and attenuators, which combine flexibility and energy dissipation to enhance protection while optimizing design efficiency. The latter will be modeled in this thesis.

The objective of this study is to further investigate the variation of the barrier's response as a function of the different possible impacts, through different sensitivity analysis: local and global sensitivity analysis carried out through the application of machine learning.

The thesis is set out in six chapters: after a brief introduction on the main purpose

of this work and general reflections on the completion of the thesis, in the second chapters an overview of the rockfall phenomena is shown with reference also to the current regulations and how to overcome its limitations. In the following chapter, it is deemed necessary to investigate the model realized in Abaqus/CAE without going into specific detail as it is not the subject of this study, but only for the sake of clarity. Subsequently, in the chapter four, the sensitivity analysis is introduced, describing its individual steps; starting with the choice of input parameters, and ending with the definition of the correlation between input and output parameters. In the fifth chapters will be explained the machine learning implementation, about global sensitivity analysis. Once the results of the analysis have been investigated, conclusions are drawn regarding the effectiveness of the completed study and any suggestions for future researchers wishing to further the study carried out in this thesis, in Chapter 6.

Therefore, as will be further explored in the following chapter, what spurs the drafting of this work is the need for greater protection of structures, infrastructures and individuals against rockfall hazards. To date, these structures have always been designed according to European standards, which, unfortunately, are not very thorough and in need of revision. In fact, current European standards, such as [1], focus mainly on the energy assessment of rockfall barriers, without providing detailed guidelines for the specific design of these structures. Furthermore, National Technical Standards often do not comprehensively address rockfall barriers, leaving a legal vacuum that can lead to different interpretations and a lack of uniformity in design criteria.

The goal of this thesis is to define a faster approach for evaluating influential parameters in rockfall phenomena in order to obtain a simplified model useful for the design of attenuators, incorporating the innovative machine learning system.

1.2 Objectives

This thesis focuses on a sensitivity analysis of the variables affecting the impact of rock blocks on rockfall barriers, aiming to better understand their interrelationships and streamline the design process for new types of barriers, such as attenuators. The present study is distinguished by the application of advanced machine learning techniques in the design of rockfall barriers, a field in which this approach is still little explored, except by means of classification algorithms useful for defining rockfall susceptibility [2]. Although machine learning has been employed in other engineering fields to optimize the design of structures, its application in the context of evaluating the responses of rockfall barriers is relatively recent. What makes this study innovative is the use of algorithms for global sensitivity analysis, which allows a wide range of scenarios to be explored quickly and efficiently, avoiding the traditional

manual approach. The implementation of such techniques could significantly reduce design time, improve the accuracy of simulations and contribute to a more informed decision-making process. In the long term, the proposed approach could also facilitate the integration of new protection technologies, optimizing the use of resources and increasing the safety of infrastructure in areas with a high risk of landslides.

The work is conducted as follows:

- Assumption of input parameters and their variation range from a scientific literature analysis. Additionally, the sampling method of the parameters is derived so that the combinations are exhaustive of the possible natural impact conditions of the blocks on the attenuators;
- Simulation of the model with the previous parameters using Abaqus/CAE software;
- Extrapolation of the analysis results for the implementation of local sensitivity analyses;
- Global sensitivity analysis is conducted to confirm previous results and improve the methodology.
- Using machine learning, a path was set to realize an algorithm capable of predicting the trend of the parameters extracted from Abaqus/CAE more quickly.

All this processes are described in the following chapters.

1.3 Limitations

Current status

The study presents several strengths as well as limitations. Its main strength lies in the simplification of certain time-consuming steps in the design of rockfall barriers. The innovative aspect of this work is the ability to automatically derive correlations between parameters influencing the rockfall process by dynamically inputting relevant variables into the machine learning algorithm, eliminating the need for manual data extrapolation and processing.

However, the current study primarily focuses on analyzing parameters related to the rock block, rather than the barrier itself, which is only superficially addressed. A deeper investigation of the interception system's parameters would require modifications to the Abaqus model, which is not part of this study.

A primary limitation stems from the limited set of parameters used, driven by the intention to simplify the model. Consequently, the findings are not entirely

exhaustive and may introduce some uncertainty. It is important to note that the aim of this thesis is not only to provide valid design results (achieved through sensitivity analysis), but also to present an algorithm capable of speeding up the design process by dynamically entering the parameters of interest, without needing to run simulations for every possible input.

Another limitation is that the simulations were conducted using a model with fixed parameters, such as slope inclination, interception net length, and net elasticity. This constraint restricts the calculations to this specific combination. However, the model remains a valuable tool that can be further improved, particularly by making result extraction from the software more versatile and less time-consuming.

Future developments

Expanding the model to include aspects of the barrier geometry and environmental parameters would make this study more comprehensive. Another crucial step would be adding dynamic variables such as seismic and climatic activity to further enhance the model's strength and flexibility. Additionally, their comparison against experimental data from the field would serve as a further step towards validating and fine-tuning the machine learning algorithms.

The model is still useful as it stands and proposes innovative approaches for expediting the design processes for rockfall barriers in well-known geological and morphological regions. It is quite evident that this type of machine learning would result in substantial time savings in the design and simulation phases, which would allow for quicker consideration of alternative treatments. It can also be used for managing risks and formulating interventions in vulnerable regions in the primary local and regional levels.

Chapter 2

Rockfall phenomena

2.1 Landslide phenomena

The professional vocabulary of geosciences defines a landslide as the distinct mass movement of slope forming materials such as natural rocks, soils, and artificial fills, among others [3]. Landslides are complex phenomena that can be categorized based on various factors. Each phenomenon is unique due to the difference in factors such as genesis and physical attributes that aid in differentiating them which makes the classification quite difficult. Eventually, geologists and researchers realize the need to establish a standard classification system. This system should include the material involved, the speed of movement, and type of movement. The classification of Cruden & Varnes presented in figure 2.1, provides for the distinction of materials into rock, debris and soil that can generate different types of movement such as falling, toppling, sliding, spreading, flow or complex movements. Each of these movements has different consequences, so it is important to analyze them individually.

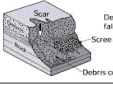
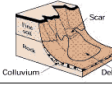
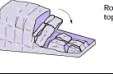
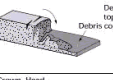
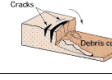
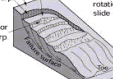
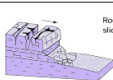
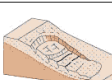
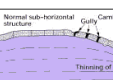
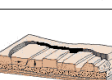
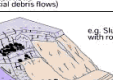
Material		ROCK	DEBRIS	EARTH
Movement type				
FALLS				
		Rock fall	Debris fall Scree Debris cone	Earth fall Colluvium Debris cone
TOPPLES				
		Rock topple	Debris topple Debris cone	Earth topple Cracks Debris cone
SLIDES	Rotational			
	Translational (Planar)			
		Rock slide	Debris slide	Earth slide
SPREADS				
		Cap rock Normal sub-horizontal structure Gully Fault Center slope structure Valley bulge structure (formed off by erosion) e.g. rambling and valley bulging		Earth spread
FLOWS				
		Soilification flows (ergological debris flows)	Debris flow	Earth flow (mud flow)
COMPLEX				
		e.g. Slump-earthflow with rockfall debris	e.g. composite, non-circular part rotational/part translational slide grading to earthflow at toe	

Figure 2.1: Table of landslides classification [4]

Furthermore, the Cruden & Varnes classification [4] categorizes landslides into seven speed classes, ranging from extremely slow to extremely rapid, visible in figure 2.2. The rate of movement significantly influences the destructiveness of the event, and this classification helps to assess risk levels.

In Italy, landslides are a widespread phenomenon due to the country's geological and morphological characteristics, with 75% of the territory being mountainous or hilly. Of the approximately 900,000 landslides recorded in European databases [5], nearly two-thirds are in the Inventory of Landslide Phenomena in Italy (IFFI project [6]), developed by ISPRA and the autonomous regions and provinces. This inventory shows that approximately 625,000 landslides are present in Italy, affecting 7.9% of the national territory. In Italy, 60,481 km², equal to 20% of the country's area, are affected by landslide warning and hazard zones.

Collapse and debris flow rapid kinematic events account for 28% of Italian landslides. Such high-speed (up to several meters per second) events are highly destructive and have a tendency to result in high loss of life, infrastructure damage, and economic disruption [7]

According to the 2021 ISPRA report on hydro-geological instability, approximately 5.7 million people live in landslide-risk zones in Italy, and almost 500,000 in very high-risk areas (P4), see figure 2.3.

Class		Movement rate	Vulnerability
Extremely slow	1	$5 \cdot 10^{-6}$ mm/sec 16 mm/y	A landslide phenomenon or landslide is extremely slow when it has velocities that are imperceptible and detectable only with appropriate instrumentation.
Very slow	2	$5 \cdot 10^{-5}$ mm/sec 1,6 m/y	Some risk elements in the area are not damaged
Slow	3	$5 \cdot 10^{-3}$ mm/sec 13m/month	Risk elements in the area may suffer moderate damage. Maintenance, repair, and reinforcement on non-vulnerable structures during downtime is possible during movement.
Moderate	4	50 mm/sec 1,8 m/hour	Risk elements in the area may suffer serious damage. The retention of some temporary and non-vulnerable structures is possible
Rapid	5	0.5 mm/sec 3 m/min	Risk elements in the area are destroyed by the impact of the displaced mass, however, the velocities allow people to be evacuated
Very rapid	6	$5 \cdot 10^3$ mm/sec 5 m/sec	Hazard elements in the area are destroyed by the impact of the displaced mass, and the difficulty of evacuation results in the loss of some lives
Extremely rapid	7		Catastrophe. Elements in the area are destroyed, and the inability to evacuate generates great loss of life.

Figure 2.2: Table of landslides classification basing on rate of movement [4]

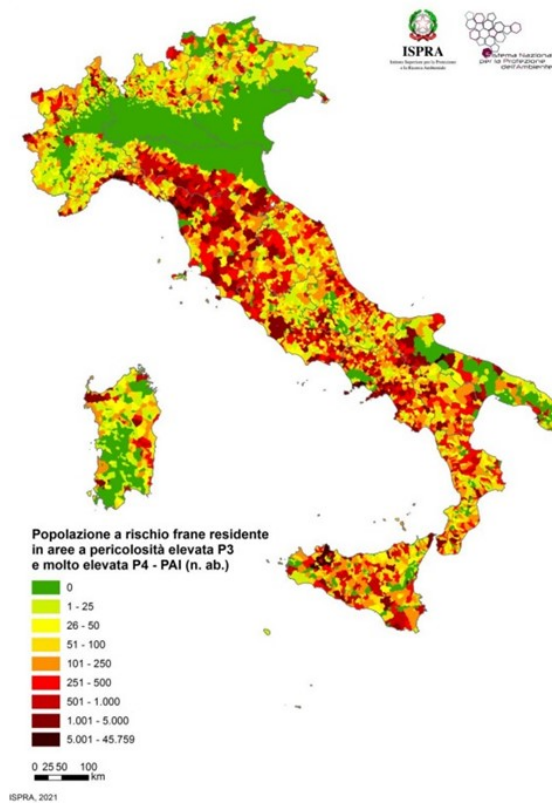


Figure 2.3: Population at risk resident in areas with high landslide hazard P3 and P4 PAI on a municipal basis (no. of inhabitants) - processing 2021 [7]

Landslide hazard is defined as the probability of occurrence of a potentially destructive event of a certain intensity within a specific area and time frame [8]. Analyzing past events is crucial for assessing hazard, but challenges arise due to the lack of detailed data on the timing of landslide triggers, making recurrence times difficult to determine. For this reason, the spatial occurrence of landslides, known as susceptibility, is often assessed.

Several Landslide Hazard Zonation (LHZ) methods exist, such as heuristic, semi-quantitative, quantitative, probabilistic, and multi-criteria decision processes [9]. These methods typically rely on landslide inventories and associated parameters. The qualitative matrix method was applied to the IFFI inventory, resulting in the following hazard mapping, reported in the following figure 2.4:

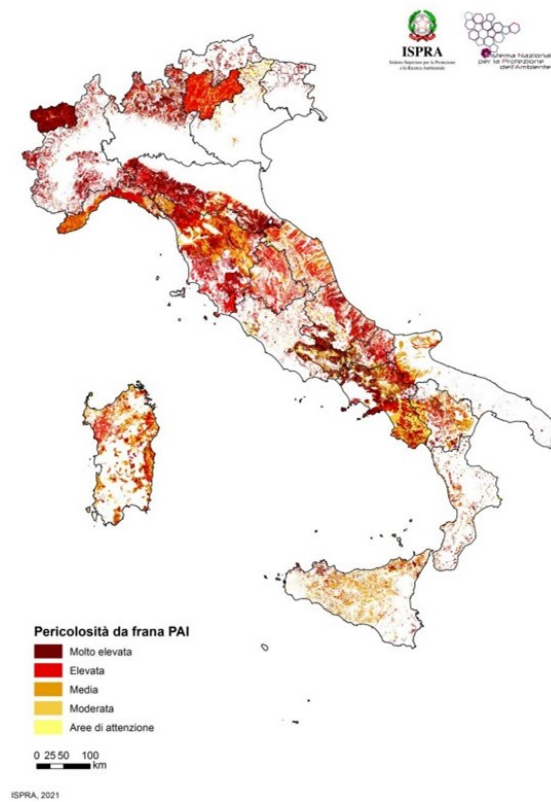


Figure 2.4: Percentage landslide index (IFFI Inventory landslide area/cell area \times 100) on mesh of side 1 km [7]

Given that the majority of Italy's territory is classified as medium to high-risk for landslides, mitigating these risks is crucial for protecting populations and infrastructure: this is possible introducing rockfall barrier protection of various types, as described in following paragraph 2.3.

2.2 Rockfall phenomena

Rockfall phenomena are widespread in many areas, including inhabited areas, which are particularly vulnerable. In these areas, the analysis of rockfall risks becomes crucial for the design of effective protection solutions.

They generally originate with the detachment of rock from a particularly steep slope along a surface with little or no shear resistance. The slopes on which they occur, in addition to being characterized by a high gradient, might be affected by the presence of structural discontinuities, such as faults and stratification planes, which may also be of neoformation. Rockfall risk analysis is a complex, multi-scale process involving several disciplines and techniques.



Figure 2.5: Rockfall events in Treviso along the provincial road 422 [TREVISO-TODAY]

The size of the blocks that can be detached is highly variable, but generally falls within the wide range of $0.01m^3$ to $100m^3$.

Thus, the possible effects on structures and infrastructures must be investigated carefully because it could be dangerous [10]. Furthermore, in the process of falling, the boulder may fragment due to the interaction between block and substrate [11]. Among the causes of detachment are all those phenomena that contribute to rock fracturing, including:

- Erosion by rainfall and chemical weathering;
- Vibration or shaking due to anthropogenic factors: explosions, roads, construction and trains;
- Fires that destroy stabilizing vegetation;
- Increased interstitial pressures due to water infiltration;
- Growth of the plant root system;

- Thawing of permafrost [12];

As well as the causes of detachment, it is essential to define the lithology and tectonics to which the survey area is subjected by observing the density of discontinuities. Sometimes the analysis starts from precursors that can define the susceptibility of the area at risk, but without being able to define the extent of the phenomenon in terms of the detachment magnitude-volume-frequency ratio, for which there are insufficient and possibly standardized historical data.

The first step to take in order to understand the phenomenon and find appropriate engineering solutions is to identify the trajectory of the blockage. It varies according to the mechanism of movement: rolling, free fall, bouncing or sliding, visible in figure 2.6.

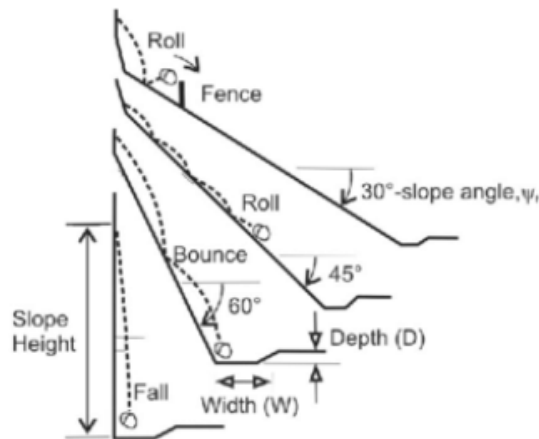


Figure 2.6: Rockfall mechanism [Neil B.]

Once the kind of movement is defined, it starts a series of simulation that aimed at knowing the possible trajectory of the block on the slope, in order to understand which point is most affected by block bounce and therefore where the most energy is manifested.

2.3 Rockfall protection structures

Rockfalls happen in rural and urban regions alike, making them the subject of interest for numerous professionals. While numerically modeling the rockfall or landslide for engineering and planning measures can be done, their spatial variability and the three-dimensional nature of the topography make it increasingly more difficult to attain an accurate risk assessment.

There are a range of approaches that have been developed to manage land and the threats it possesses. That said, the methods differ greatly in the level of research or analysis detail required, the objective of the study, and the scale of the analysis. One common classification of various types of rockfall protective measures attempts to categorize them in two broad groups:

- **Active structures**

They intervene at the origin of the problem by preventing the detachment of stone elements from the slope:

- Interventions that modify the rock mass mechanical resistance;
- Interventions that act on the surface of the rock mass;

- **Passive structures**

They intercept or deflect boulders that have been mobilized with structures mainly located at the base of slopes or rock faces. The main kinds are listed here and shown below in figure 2.7 :

- Installation of rockfall barriers;
- Earth embankments (reinforced or not);
- Adhesion nets and cortical reinforcements.

The choice between these types of countermeasure is mainly governed by the kinetic energy of the block and the topographic constraints [13].

Rockfall slides are unique to each location and therefore pose a challenge when trying to understand and analyze them. Using a variety of methods, geologists need to determine the equilibrium of the rocks and foresee the movement of the rocks.

In scenes of uncontrolled rockfall, the most frequently undampened measures applied to prevent rockfalls are net fences. These measures were detailed in Chapter 2, for explanation of these fences as barriers see Chapter 3].

2.4 New types of protection structures

Although many traditional solutions exist, new types of barriers have emerged over the past decade that combine efficiency and practicality, reducing costs and increasing durability. Among these, hybrid barriers and attenuators are proving to be among the most promising. These systems are advantageous compared to their predecessors, because they combine the energy absorption typical of classic barriers with the reduced maintenance typical of inadherence nets [14].

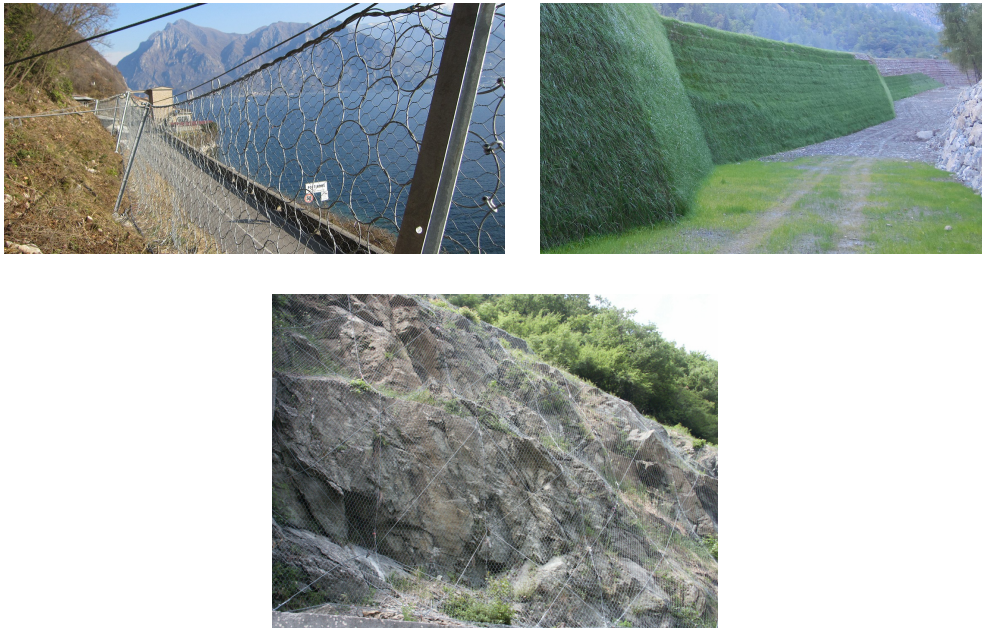


Figure 2.7: Rockfall protection barriers:

- (a) Net Fence [IncofilTech]
- (b) Earth embankment [Tenax]
- (c) Inhaderence net [BorghiaZio]

Hybrid barriers and attenuators can be classified as passive, flexible barriers; they are characterized by a wire mesh with a ring or cable weave, suspended from an upper horizontal support cable raised from the surface of the slope by posts or suspended from anchors through a chute. It is often preferred to limit the presence of lateral anchors in order to increase the flexibility of the barrier.

What differentiates a hybrid barrier from an attenuator (example in 4.13 is their performance in relation to the impacting block's kinetic energy dissipation [14].

The advantage over the use of classical barriers is mainly in the simplicity of installation and maintenance: these are 'self-cleaning' barriers, as already described, they simply accompany the boulder to the foot of the slope. Installation, on the other hand, can also take place further up the slope, not increasing maintenance costs, but rather giving the opportunity to capture boulders with greater energy by means of less robust, and therefore cheaper, barriers.

Although often collectively referred to as "hybrid barriers," attenuators and hybrid barriers are distinct and should be differentiated.

Hybrid barriers resemble classical rockfall barriers but feature a larger net that is not flat but rather draped. Their primary function is to completely reduce the kinetic energy of a falling boulder and guide the block down slope to a collector.



Figure 2.8: View of prototype attenuator system installed in Stanwell Park by Geobrugg [13] [GeoBrugg]

Hybrid barriers are strategically placed close to storage areas so that the draped tails direct the boulders toward the intended location.

Attenuators, as analyzed in this study, feature an opening at the bottom. Their purpose is not to stop the block entirely, but to reduce its kinetic energy so that it reaches the foot of the slope with reduced speed and different trajectory. The rocks are collected in specific trenches. Typically, these barriers are installed in series to protect a larger area, thus preventing material accumulation at the foot of the slope from becoming localized. The attenuators are located away from infrastructure, with the panel length being variable, and this is part of the study focus.

2.4.1 Essential elements of innovative rockfall barriers

The structure of hybrid barriers and attenuators is similar to that of classical rockfall barriers, which are described in detail in this chapter. However, the innovative systems consist of three distinct zones, shown in figure 4.13:

- Interception Area [A]
- Rock Bounce Control [B]
- Collecting Area [C]

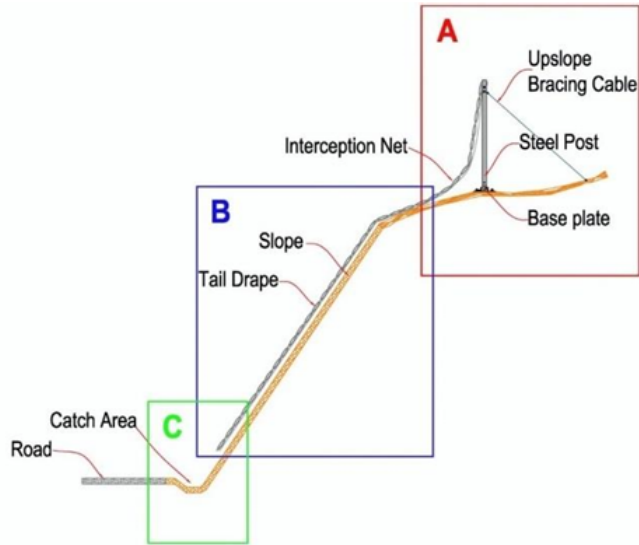


Figure 2.9: Attenuator main zone [14]

The first zone, Interception Area [A], consists of the barrier itself, which intercepts the boulder and absorbs much of its kinetic energy, deforming elastically or plastically. This phase, along with the second phase, reduces the rebound height of the block, ensuring more contact with the slope for better conveyance.

The second zone, Rock Bounce Control [B], is responsible for guiding the block down the slope while dissipating its energy to overcome friction with both the ground and the net. The effectiveness of this phase depends not only on the type of barrier and the size of the detached rocks but also on the nature of the soil on the slope. The length of the drape in this area is sized according to the expected energy to be dissipated.

Finally, the third zone, Collecting Area [C], is where the block, now with minimal kinetic energy, comes to rest. This can be achieved by using a ditch, trench, embankment, or another barrier, preventing the material from encroaching upon the protected infrastructure.

There are two main categories of rockfall barriers:

- **Barriers with limited deformability:** the rock impacts on the net, which dissipates energy by deforming. They are generally made of reinforced concrete or metal gabions, often supported by buttresses and anchored to the ground.
- **Highly deformable barriers:** they use energy dissipators, such as steel rope rings with friction blocks, to absorb higher impacts. They are easy to install and maintain and represent the type of barrier studied in this thesis.

The following figure illustrates the reference model:

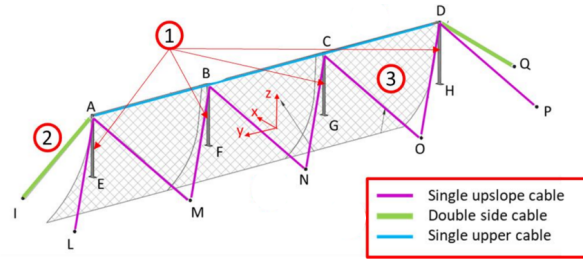


Figure 2.10: Model to be implemented in Abaqus/CAE [Courtesy of Carriero MariaTeresa from her PhD thesis (in submission)]

The characteristic elements of elastic rockfall barriers are:

- *interception structure*;
- *posts*;
- *cables*;
- *dissipation elements*;
- *connection elements*;
- *foundations*;

The *interception net* (see figure 2.11) must withstand the impact of the block by deforming first elastically and then plastically. It is made of galvanized steel and can be reinforced with vertical or horizontal ropes. The net configuration is representative of structural strength and is modelled in Abaqus/CAE as a four-node shell with finite membrane deformations.

The *posts* are steel structures (tubular or metal profiles) connected to the foundation by hinges to dissipate part of the impact, as shown in figure 2.12. They are rigid elements that must resist in the event of a direct impact, even if the probability is small. The connection between uprights and the net occurs through special elements capable of dissipating part of the energy generated in the impact. They are modelled in Abaqus/CAE with non-linear elastic-plastic behaviour, considering isotropic behaviour.

Concerning *cables*, there are different types of them, for clarity, in this work, they will be called:

- Single upslope cable: to keep in the right position the net;



Figure 2.11: Detailed representation of interception structure [risp-rockfall protection]



Figure 2.12: Detailed representation of posts [Geoflum]

- Double side cable: to connect the net with the foundation;
- Single upper cable: to keep stretch the net.

The second ones transfer the impact forces to the ground and therefore must be sized taking into account the maximum load for which the barrier is designed. It is denoted that these elements were constructed as two-dimensional elements steel made.

The *cables* are generally connected to *energy dissipation devices*, represented in figure 2.13, activated when the mesh exhausts its absorption capacity, they transform impact energy into plastic work through deformation. These are positioned both in the anchor ropes and in the longitudinal ones; they are essential for energy dissipation even in non-perpendicular impacts. There are many types and therefore careful analysis is necessary case-by-case evaluation.



Figure 2.13: Detailed representation of dissipation elements [Maccaferri]

Connecting elements and foundations: they transmit stresses to the base structure, which generally consists of concrete micropiles connected by steel plates. The figures represent hybrid barriers, but the constituent elements are the same as those used for attenuators, with the difference already shown in 2.11, which concerns the stiffness imparted to the interception system.

2.4.2 Hybrid barrier and attenuator design

Despite these are two fundamentally different systems, there are common steps in their design. In general, what needs to be considered is:

- Definition of input data for the design;
- Calculation of the dynamic impact on the barrier and selection of the barrier;
- Evaluation of the static load on the barrier.

The modelling of the phenomenon begins with the investigation of the morphology and topography of the slope that have an influence on the block trajectory and rebound heights. From this analysis, input data are extracted regarding the

characteristics of the block; it is the objective of this study to understand the influence of the input parameters on the response of the barrier (see chapter 4). In addition to geological data, it is needed to carry out the study of the trajectories by means of special software and finally a back analysis on the previous data concerning rockfall phenomena. The study of trajectories is fundamental to define the point of arrival of the block in situ or the area where it is most likely to pass, in order to establish the most efficient position of the barrier.

There are different methods used to analyze rockfall energies and trajectories whose objective is to quantify block velocity, impact energy and impact height, which are key input parameters of this analysis. All these approaches are based on, to differing degrees, actual field rock rolling data, and are used as tools to assist in the design and the assessment of mitigation measures. Where possible, all these methods should be used to analyze the rockfall trajectories at the site [15].

To achieve this goal, over time, many full-scale in-situ tests have been realized, although expensive, provide real data that are crucial for barrier design. However, the evolution of technology and software has made it possible to simulate these scenarios, cutting costs and allowing a faster and more detailed evaluation of various parameters. A further advantage of using software is the possibility of investigating a higher number of parameters such as speed, energy and plasticity of the tested structures. It is precisely this saving of time and money that is the focus of this thesis, the ultimate goal of which is to obtain a machine learning algorithm that can predict the variables at play under conditions of block impact on rock and consequently speed up design time.

The models to be implemented can be structured in various ways, choosing to use a rigid-body model such as the "lumped-mass" model, or hybrid models. The study carried out in this thesis involves the first type of model, which will be explained in detail in chapter 3. After that it is necessary to investigate the kinetic energy with which the block moves. In particular, it has formulation:

$$E_k = \frac{1}{2}mv^2$$

knowing that m is the mass of the block and v its velocity defined at a specific point in its trajectory.

To define the correct type of network to use, it is necessary to equalize the kinetic energy found with the work done by a constant force F to blocking it. Based on the displacement s , given by the path of the blockage, it will be possible to identify the F and thus the most suitable barrier.

$$E_k = \frac{1}{2}mv^2 = F * s$$

By getting a time interval, established by [1], and comparing the force required to capture blockage by flexible and hybrid barriers, it was concluded that the force required by hybrid barriers is always lower than by flexible barriers. Despite these conclusions, it is noted that it is impossible to know exactly the loads applied on the barrier. Therefore, it is recommended to always use additional energy dissipation tools, characteristic of flexible barriers, even for hybrid barriers, to be conservative [14].

Having identified the type of barrier, it is essential to make sure that it can withstand the static loads following the landslide phenomenon, characterized, for example, by debris accumulation, snow accumulation, and net weight. Static loading is generally lower than dynamic loading, unless one is in special situations such as:

- very long net tail, greater than 50 m;
- steep slopes, sloping more than 70°;
- high amount of debris under the drapery.

So, through this analysis it is possible to make sure that the tensile strength of the main mesh is sufficient to bear the static load and to choose the number of longitudinal ropes required, and their sag, to avoid the static loads activating the energy dissipater device.

2.5 Rockfall barriers legislation

Currently, design of rockfall barrier systems largely focuses on the certification of barriers with respect to their ability to resist a target energy, as put forward by the requirements stipulated for the certification in the European Assessment Documents [1]. The principal design is simply ensuring that barriers have the ability to absorb and dissipate target expected impact energy so as to safeguard road users without being over the existing regulation.

However, despite the increasing popularity of new technologies for rockfall protection, there is still a general lack of information and consensus on the design specifications of certain systems, particularly attenuators. Unlike traditional barriers that merely stop rockfall, rockfall attenuators are designed to reduce the energy transferred to the barrier and underlying infrastructure, typically by utilizing mesh or netting systems combined with damping devices. While empirical testing protocols—such as those used by the Colorado Department of Transportation, "Colorado's full-scale field testing of rockfall attenuator systems"[16]—have been developed to guide designers, an overall, internationally accepted methodology for the entire design process of attenuators is in the process of being developed [14].

Within this chapter, the current regulatory framework and the method of defining the safety factor for rockfall protection systems will be examined, examining the innovations that reliability analysis could take to attenuator design.

2.5.1 European Normative

Designing rockfall protection barriers, such as attenuators, is heavily governed by European standards that provide the safety and performance criteria. The most suitable regulation in this context is EAD 340059-00-0106, which was introduced in 2009 with name (ETAG027) and provides the methods for the inspection of rockfall barriers as protective systems. According to this document, their performance needs to be checked based on key properties such as the energy-absorbing capacity, height, and maximum elongation of nets. But this specification is only dealing with traditional rockfall barriers, and attenuators may require special considerations, since they contain elements specifically designed to absorb impact energy rather than just intercepting material.

ETAG 027 was replaced in 2018 by the European Assessment Document [1], which combines the findings of field tests and provides a new way of determining the performance of protective systems. The transition to EAD represents a coming together of the findings gained through intensive testing conducted from 2009 to 2018, despite the fact that there remain a few gaps in research, particularly in terms of rockfall attenuators' performance in specific circumstances. The guidelines of EAD [1] mention energy dissipation mechanisms but do not have specific methodologies for attenuators that might require investigation through more fine-tuning of available test methods. The complete evolution of the standardization of rockfall barrier testing is described in [17].

Another important regulatory system is the Eurocode 7 (EN 1997-1:2004) [18], addressing the geotechnical design of structures. As part of the overall Eurocodes, it provides guidelines to ensure stability and safety in geotechnical systems, including those used for protecting against rockfall. While Eurocode 7 is based on the Limit State Design (LSD) philosophy, a semi-probabilistic method where partial factors have been employed to capture uncertainties in loads and resistance, the main focus is laid on traditional barriers, with attenuators typically deserving special consideration.

Italian design aim to validate the safety and effectiveness of rockfall defense equipment: UNI 11211 standard of UNI in 2012 [UNI-11211], currently revised, addresses all types of rockfall defense works, including attenuators. The standard specifies the design philosophies to be utilized, even if remain practical aspects and open issues in the application of these standards [17].

For instance, EN 1990:2002 outlines the general rules for the design of structures, but some challenges in the design of rockfall net fences have recently been addressed

using a time-integrated, reliability-based approach [19]. In addition, novel design techniques like the Finite Element Method (FEM) and the Discrete Element Method (DEM) have proved useful in the analysis of the rockfall impact-interaction with the protection systems. These advanced methods are essential to attenuator design since they allow for more accurate modeling of the energy absorption and dissipation by netting systems and damping elements [20]. These software packages are increasingly being incorporated into rockfall protection designs in an effort to refine both the accuracy of energy transfer calculations and the functioning of the protection systems as a whole.

However, a key challenge remains: the vast amount of data generated by these simulations. To address this issue, artificial intelligence (AI) has been employed to mimic the behavior of complex models and account for multiple variables—such as impact angle and point of impact—that are not currently considered in traditional evaluation procedures. These mathematical tools, although effective, are typically constructed for specific types of barriers and do not fully incorporate site specificity, which is essential for a more accurate and tailored design approach [21].

2.5.2 Current and future design methods

The deterministic approach used today in Limit State Design (LSD) is constrained, especially with regard to the uncertainties of the inherent rockfall event—such as size, velocity, and impact angles of boulders. Due to these difficulties, reliability analysis, a probabilistic approach that allows for further consideration of such uncertainties and better quantification of the risks of rockfall impact, is gaining greater attention.

The fundamental assumption of LSD, that the **action values** (forces transferred by rockfall on the barrier) must be less than the **resistance values** of the structure, remains valid. It is now better understood that the deterministic method of LSD may not be fully adequate for structures like attenuators. The action value E_d and the resistance one R_d must be evaluated in a probabilistic framework where safety factors and uncertainties on both the action (rockfall impact) and resistance (barrier capacity) are taken into account. This gives a more robust and flexible procedure, especially for attenuators under highly variable impact loads.

In the last decade, an increasing number of studies have investigated integrating reliability analysis in rockfall barrier design, specifically in the response of attenuators under different types of rockfall events. Although partial safety factors are able to compensate for uncertainties in conventional designs, they cannot deliver detailed information regarding the likelihood of failure, particularly for attenuators that use energy dissipation via intricate mechanisms. Therefore, the application of reliability-based design methods is becoming more significant for attenuators since they are better able to deal with material property and environmental condition

uncertainty [22].

In addition to reliability analysis, advanced computational methods, such as numerical modeling, need to be incorporated to optimize the design of rockfall attenuators. Finite Element Analysis (FEA) and Discrete Element Modeling (DEM) can simulate the performance of rockfall interaction with attenuators in greater detail, which gives a better prediction of energy absorption and dissipation [20].

Despite these advances, there are still difficulties in applying these methods to all site-specific conditions. One of the directions for resolving these difficulties is the use of artificial intelligence (AI), as AI can be employed to refine attenuator designs by analyzing vast amounts of simulation data and considering site-specific parameters, such as terrain and rock type, which are typically difficult to incorporate in traditional methods.

Overall, while rockfall attenuator design remains in an evolving phase, a combination of probabilistic reliability analysis, computational modeling, and AI-based methods will significantly enhance the effectiveness and safety of the systems in the future times.

Chapter 3

Numerical Modelling in Abaqus/CAE

3.1 Software introduction

Abaqus/CAE is an advanced finite element analysis (FEA) software designed to simulate complex problems in various engineering fields. It can perform both simple linear analyses and advanced nonlinear analyses, making it suitable for the study conducted. It is therefore possible to model any physically reasonable combination of elements, materials - also able to simulate geotechnical materials such as soils and rocks - procedures and loading sequences. Abaqus/CAE is the Complete Abaqus Environment that provides a simple interface for model creation. The software is structured in modules that manage the different phases of the modelling process: pre-processing, simulation and post-processing, as illustrated in the figure below:

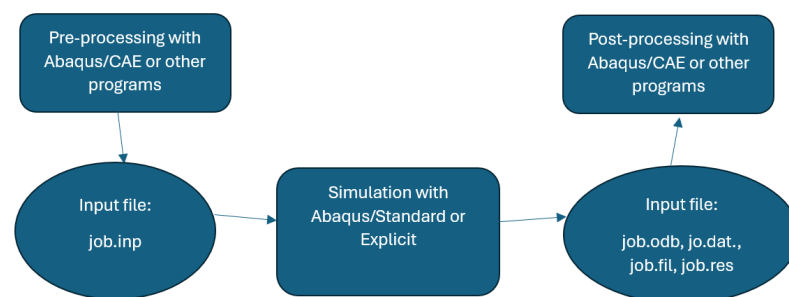


Figure 3.1: Example of flowchart in Abaqus/CAE

Model Implementation: From Concept to Simulation on Abaqus/CAE

In accordance with the previous section, the flowchart designed for the implementation of the model under study, is here shown:

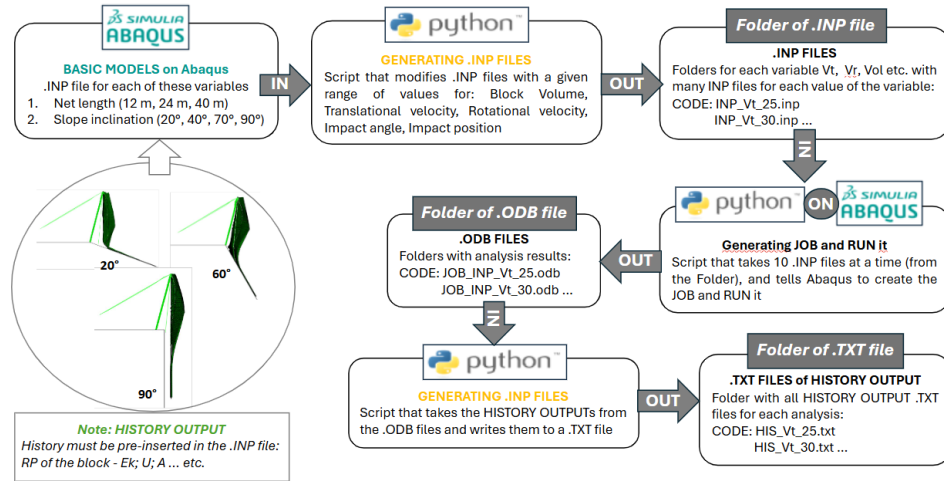


Figure 3.2: Implemented flowchart in Abaqus/CAE [Courtesy of Carriero Mariateresa from her PhD thesis (in submission)]

Knowing all the physical aspects of the problem to be analyzed, it is possible to implement them within the chosen program. In order to optimize the computational costs, it was decided to work in the Python language. The drafting of the codes used is not the subject of this thesis, but reference is made to [23] for more details.

In this study, the same procedure was followed, using the codes provided already compiled, in order to carry out further analysis on the simulation's results.

3.2 Model geometry

An Abaqus/CAE model consists of a collection of elements that, when assembled, represent the physical problem to be solved and the solution to the analysis. The basic components of the analysis are: geometry, section properties, elements and materials, loads and boundary conditions, analysis type and output requirements. To implement the model, all the elements described in 2.4.1.

The basic geometry is defined using finite elements and nodes. Each element is a separate component of the structure, connected with others by nodes, forming the mesh, which is the discretization of the actual geometry of the system analyzed. The density of the mesh directly affects the accuracy of the simulation: a denser mesh improves the accuracy of the results but increases the time of calculation. In general, the solution obtained is an approximation of physical reality and the quality of the model determines its reliability.

The structure employed is the model presented in 2.4.1 with all its components, placed on a slope inclined of 45° . To examine different deformation shapes of the network, the slope's inclination was changed in this analysis. The actual model consist in 60° inclination angle. The terrain profile is demonstrated in the following figure 3.3.

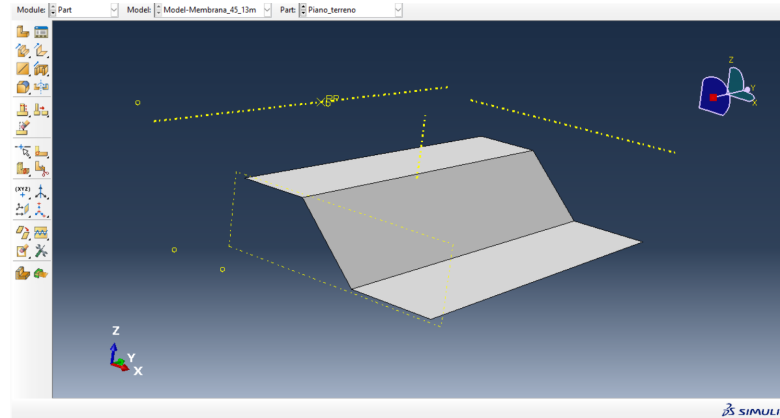


Figure 3.3: chosen geometry of ground surface in Abaqus/CAE

All the net elements are mounted in reproducible modules to form a barrier adapted to external conditions, capable of effectively opposing rock collapse phenomena. An example of a complete structure is illustrated in the figure below:

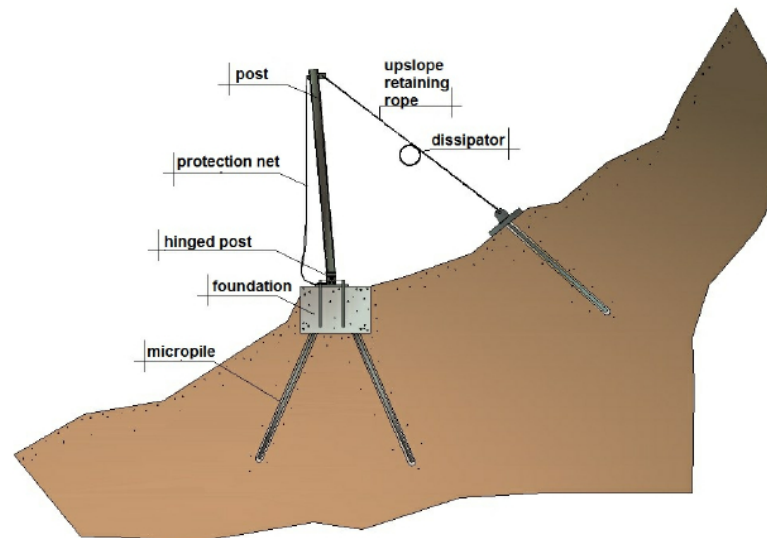


Figure 3.4: rockfall barriers [Geostru]

The model creation also requires identifying the shape and geometry of the

rock block. Since the block morphology evolves with numerous parameters with respect to detachment, we assume an rigid body with elongated shape and square cross-section similar to a gyroscope, as shown by the figure below.

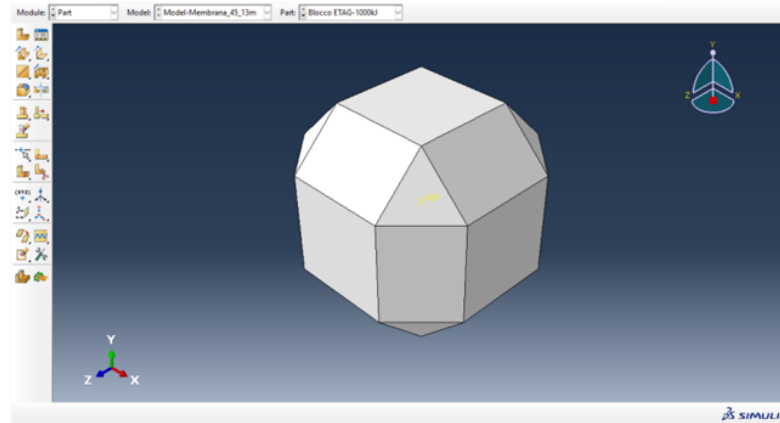


Figure 3.5: selected rock block geometry in Abaqus/CAE

For the purpose of a realistic analysis, isotropic material behavior is presumed and the rhombicuboctahedron shape was chosen to correct the unrealistic spherical shape.

Abaqus/CAE is a powerful software that has been used in different studies to simulate complex geotechnical processes like mechanisms of rockfalls. It was used, for example, for evaluating the performance of rockfall barriers in different geological contexts and investigating the dynamic impact response of protection structures. The finite element approach allows simulating in detail the interaction between rock blocks and barriers, providing useful results to design and optimize hazard mitigation systems [24].

The final result of the model, with all the parts described, is presented in figure 3.6.

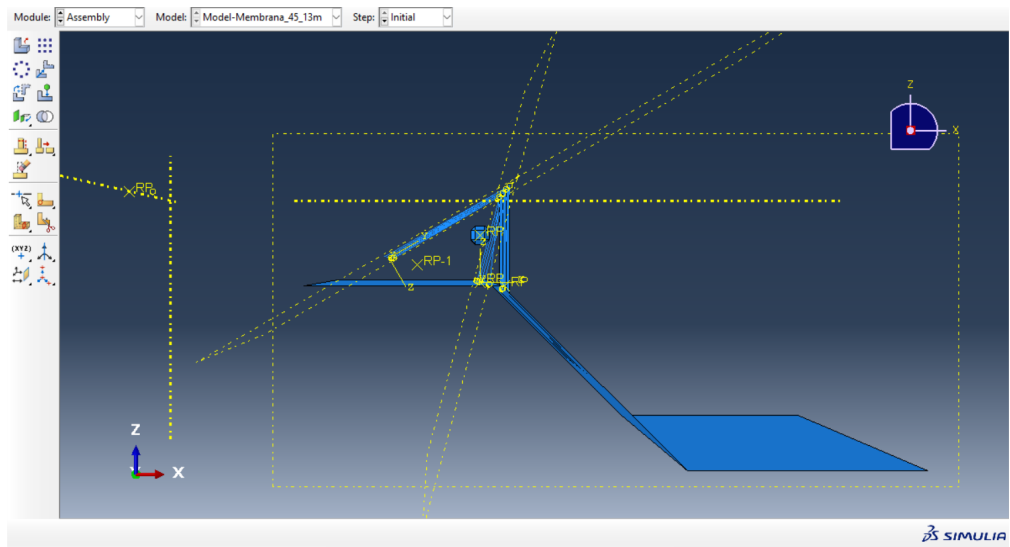


Figure 3.6: Side section of the entire structure in Abaqus/CAE

Further details on the model can be found in [23].

Chapter 4

Sensitivity analysis

In sensitivity analysis, various methodologies exist, all aiming to assess the influence of input variables on each other. These methods help identify critical factors, enhance model understanding, and improve confidence in the results. The most common approaches include:

- **One-at-a-Time Analysis (OAT) or Local Analysis:** Varies one input at a time while keeping all others constant, recording its effect on the final result.
- **Morris Method:** A systematic extension of OAT, selecting multiple input combinations to evaluate individual variable effects.
- **Global Analysis:** Varies all inputs simultaneously within defined limits to assess their combined impact.
- **Sobol Method:** A global analysis technique that decomposes output variance to quantify each input's influence and interactions.
- **Analysis of Variance (ANOVA):** Assesses the significance of each input and their interrelationships by decomposing output variance.
- **Scenario Analysis:** Studies specific input combinations rather than systematically varying them, often used in 'best-case – worst-case' evaluations.

This thesis applies two of these methodologies:

- The **One-at-a-Time Analysis**, described in this chapter.
- The **Global Analysis**, implemented through a Python-based machine learning algorithm (see Chapter5).

4.1 Selection of input parameters

The analysis of the model described in the previous chapter can be carried out in visual mode, through the Abaqus/CAE interface with which one can observe the evolution of the blocking process on the network via the ‘result’ command. However, considering the large amount of data taken into account for this study, it was preferred to carry out an analysis using Python codes. Following this way, time can be reduced considerably.

From literature research and because of past experience, the following parameters were identified as fundamental to be given as input to the system:

- Block volume [m^3], determines the mass and inertia of the falling rock;
- Translational velocity of the block [m/s], represents the linear speed at which the block impacts the net;
- Rotational velocity [rad/s], accounts for the block’s angular motion, which influences impact dynamics.
- Impact angle on the net [$^\circ$], the inclination at which the block strikes the net, affecting energy dissipation;
- Impact position along the vertical and transverse direction of the network, influencing load distribution.

Volume, shape and unit weight of the block are derived from analyses of the degree of fracturing of the rock mass.

Using previous studies and practical experience, appropriate value ranges were established for each parameter. These ranges define the variability of inputs used in the simulations and are summarized in the following table. 4.1:

Volume	Translational velocity	Rotational velocity	Impact angle	Impact position (Y)	Impact position (Z)
$1.21m^3$	$25m/s$	$0rad/s$	20°	$0m$	$3m$

Table 4.1: Basic set up for parametric analysis

These values were set and then individually one parameter at a time was changed in order to understand the effect each parameter had on the others. On the other hand, the following values were established and set for slope and network characteristics: At this point the sensitivity analysis was started.

4.2 Local sensitivity analysis

Sensitivity analysis is a valuable tool for assessing how input parameters influence the behavior of a studied system. In this research, it plays a crucial role in

Elasticity	Slope inclination	Panel length
$1.01 * 10^6$ Pa	60°	$6m$

Table 4.2: Slope and net characteristics

developing an algorithm capable of simulating the response of a highly complex model—specifically, a rockfall barrier—where multiple interdependent variables must be considered. Unlike assuming predefined parameter distributions, this study takes an empirical approach, complementing a parallel thesis [23].

To begin, a local sensitivity analysis was performed by systematically modifying individual parameters and evaluating the corresponding changes in the simulation outputs generated in Abaqus/CAE. This analysis was initially conducted using thirteen different parameter combinations, where each parameter from Table 4.1 was varied one at a time.

Subsequently, an additional six combinations were introduced, incorporating modifications to the parameters listed in Table 4.2.

The final set of parameter combinations used in the sensitivity analysis is summarized below:

PARAMETERS	BASIC SETUP	VARIATION
Panel length [m]	13	18, 40
Slope inclination [°]	60	20; 90
Panel Deformability [Mpa]	100	25; 230
Block dimension [m] (Volume [m ³])	1.2 (1.21)	0.5; 1.5 (0.09; 2.4)
Traslational velocity v [m/s]	25	10; 30
Impact angle α [°]	20	-20; 0; 40
Impact height z [m]	3	1.5; 4.5
Impact position in central module y [m]	0	2.5
Rotational velocity ω [giri/sec]	0	-3; 3

Figure 4.1: Variation of chosen parameters

The need to understand the influence of some parameters on others stems from the desire to create a simplified model of the rockfall barrier to make design more effective and less wasteful. Therefore, once the simulations were carried out on the Abaqus/CAE software, the results were extrapolated, during time, in terms of:

- Block acceleration during time to define the maximum deceleration value a_{max} (see figure 4.2);

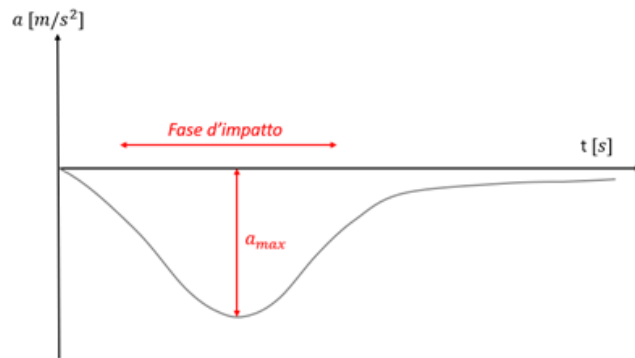


Figure 4.2: Schematic definition of a_{max} [Courtesy of Carriero MariaTeresa from her PhD thesis (in submission)]

- Displacement of the central point of the upper cable to define the maximum deflection value f_{max} ;

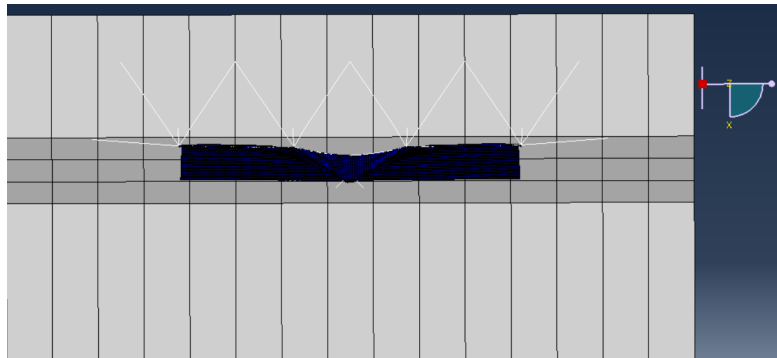


Figure 4.3: Abaqus representation of interception net, view from above

Carefully looking at the figure 4.3, one can see a deflection of the upper cable, which is shown schematically in the following diagram (figure 4.4), in which the black line represent the upper cable and the maximum displacement is called f_{max} :

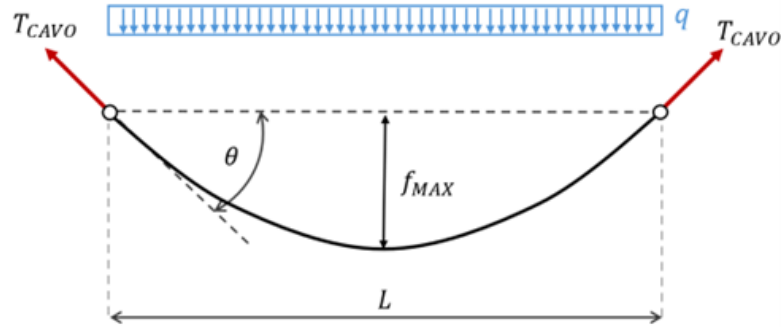


Figure 4.4: Analysis diagram for the upper cable [Courtesy of Carriero Maria Teresa from her PhD thesis (in submission)]

From the analysis diagram shown, it can be seen that the upper cable is represented by a suspended inextensible rope, stressed by a uniformly distributed load q , according to the diagram below. The maximum deflection f_{max} in the centre is plausibly useful for determining the tensile action in the upper cable T_{cavo} and its inclination θ in the panel plane in the impact condition.

- Temporal variation of the kinematic conditions of the block ($a_x, a_y, a_z, v_x, v_y, v_z, u_x, u_y$ and u_z);
- Energy variation starting from the kinetic energy of the block;
- The angle α indicating the portion of the block that contacts the panel, as shown in figure 4.6

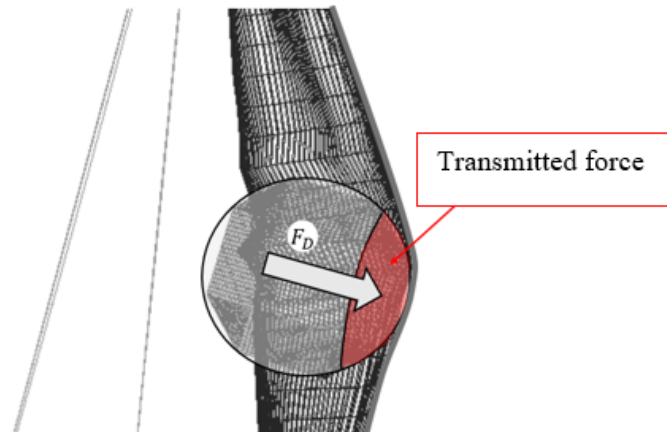


Figure 4.5: Diagram of the portion of the sphere in contact with the barrier during impact [Courtesy of Carriero Maria Teresa from her PhD thesis (in submission)]

The force F_d is considered to be transmitted to the contacting portion of the panel as a uniform pressure normal to the membrane (see Figure 4.5). The pressure (p) distribution induces tensile stresses tangent to the sphere in the membrane along the boundary of the block-panel contact zone (t), clear in figure 4.6, where it is possible to observe the α angle searched:

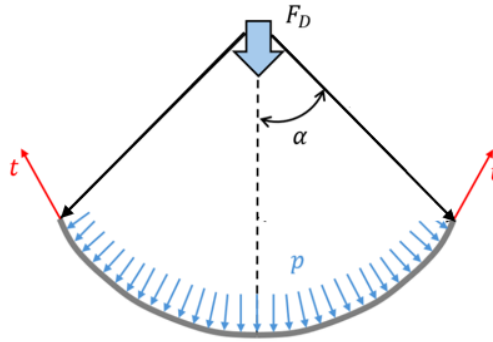


Figure 4.6: Scheme for α representation [Courtesy of Carriero Maria Teresa from her PhD thesis (in submission)]

- Net stresses (but it is not the main focus of this thesis).

The extracted results are presented graphically over time. As an example, the basic setup is illustrated below in Figure 4.7 and the following ones.

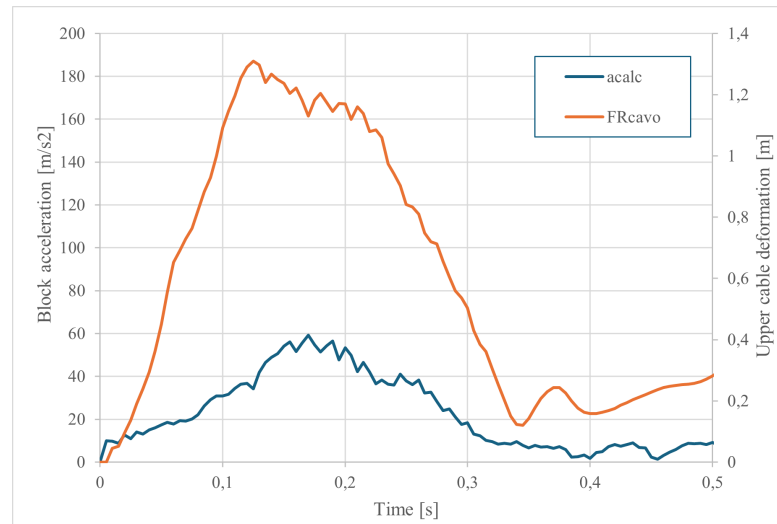


Figure 4.7: Block acceleration VS Upper cable deformation

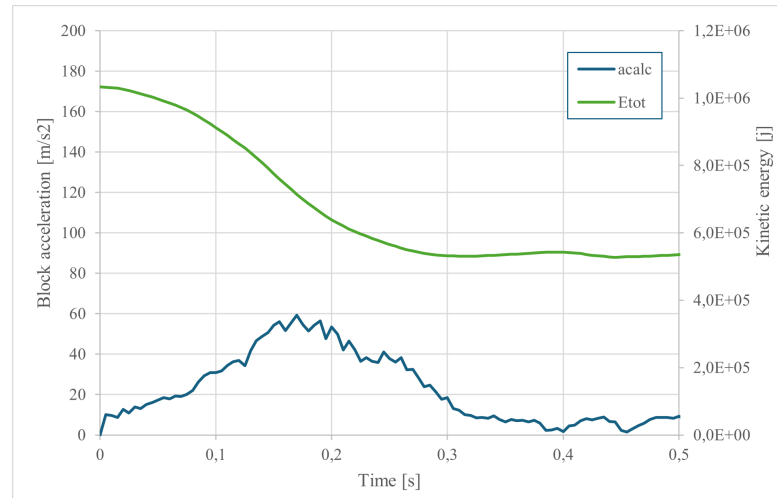


Figure 4.8: Block acceleration VS Kinetic energy during time

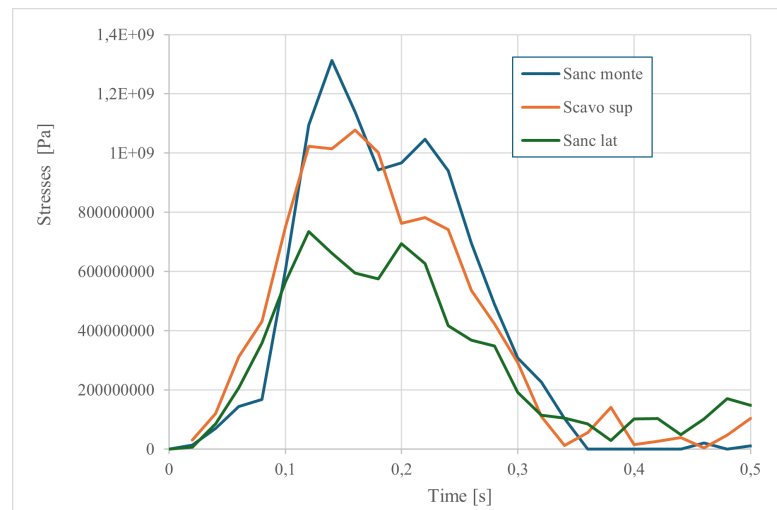


Figure 4.9: Net stresses during time

Based on the graphs, the impact instant was set at **0.15 s**, as it corresponds to the highest acceleration value and aligns with the peaks observed across different graphs. The key correlations between each parameter and the obtained results were then analyzed.

To streamline the analysis, these comparisons were integrated into a machine learning algorithm. Once the findings from the local sensitivity analysis are presented, they will be compared with the results of the global sensitivity analysis conducted using machine learning.

4.2.1 Volume

At that fixed time, different combinations were compared and the following results were extracted:

Acceleration

To estimate the maximum transmitted deceleration force, the condition of maximum deceleration a_{max} is considered. The analysis reveals an inverse proportionality between volume and impact acceleration: as volume increases, acceleration decreases.

For simplification, external influences such as slope morphology are neglected, focusing solely on the intrinsic relationship between these parameters.

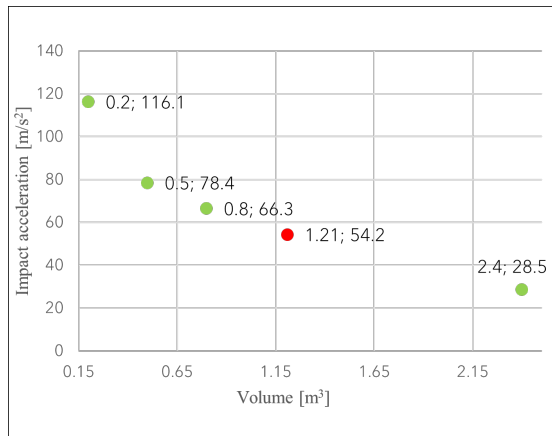


Figure 4.10: Relation between Impact acceleration and Volume of the block

During the impact phase, the purpose of the intercepting panel is to dissipate the energy of the block by deformation. The block undergoes deceleration by transferring an action to the portion of the panel that comes into contact with it. So, according to the second law of Dynamics expressed by Newton, the decelerating force experienced by the block upon impact will be:

$$F_d = m * a$$

It is known that the relationship that binds volume (V) and mass (m), by means of density (ρ) is:

$$\rho = \frac{m}{V}$$

This means that, for the same braking force, volume and acceleration must be inversely proportional, as the graph shows the relation is $V \propto \frac{1}{a}$.

Upper cable arrow

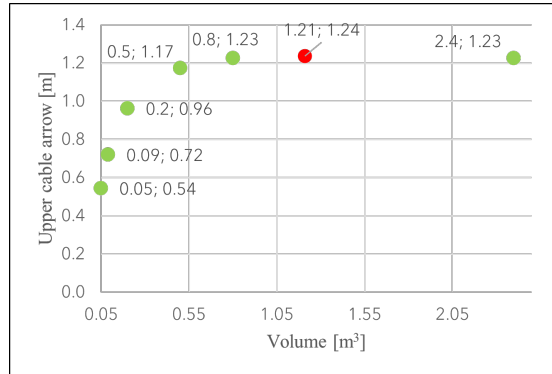


Figure 4.11: Relation between Deformation of the upper cable and Volume of the block

In contrast to acceleration, the change in the magnitude of the displacement of the top wire of the net (see 3.2) they are directly proportional ($V \propto f_{max}$). The greater the volume of the block, the greater its size, so it is to be expected that greater net deformation will result.

Kinetic energy

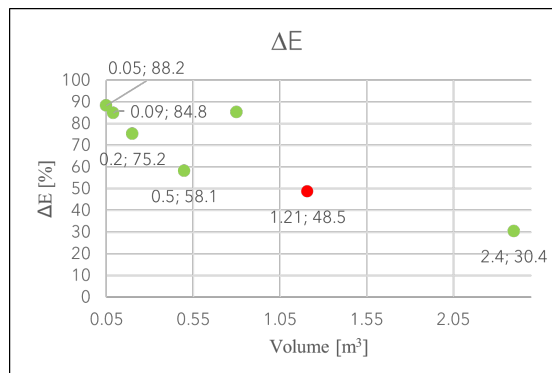


Figure 4.12: Relation between Energy variation during the impact and volume of the block

To understand the variation of energy as a function of volume, consider the relationship:

$$E_k = \frac{1}{2}mv^2$$

For which the same relation in 4.2.1 is valid, thus energy and volume grow together ($V \propto E_k$). Shown in the figure is the change in energy (ΔE), calculated as Kinetic energy at time equal to 0.5 seconds minus its value at time 0, i.e. initial. Always neglecting secondary effects related to, for example, the interaction of the block with the ground, it must be taken into account that a greater volume implies less rotation and therefore less energy waste. In addition, an important consideration must be made with regard to the size of the block, so that the contact surface of the block on the mesh increases with volume, density being equal, so that the kinetic energy of the block has more space to distribute, reducing the localization of stress and therefore its dissipation in the form of mechanical energy.

Stresses on net cables

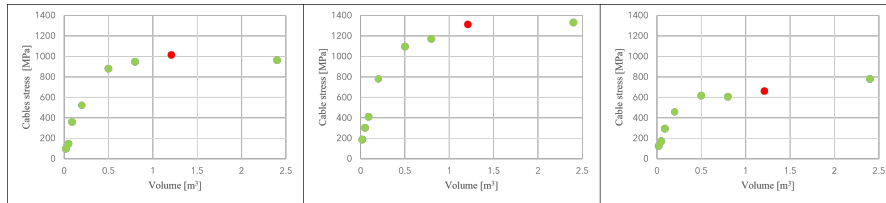


Figure 4.13: Relation between stresses on the cables and the volume of the block

The kinetic energy of the block (5.1) determines the force transmitted to the barrier during impact, which can be calculated as:

$$F = \frac{\Delta p}{\Delta t}$$

if $\Delta p = mv$ is momentum change and Δt is the contact time with the barrier. So there is a direct proportionality between the applied force and the mass, hence the volume of the block ($V \propto F$): larger blocks correspond to a greater force that can be translated in stresses so ($V \propto \sigma^2$). The stress relief that is noticeable for larger volumes depends on the fact that the greater the block, the greater the distribution of the impact force on the various cables, consequently decreasing the impact on the individual. However, this is only a hint at the reaction of the structure to impact because it is not the subject of this discussion; the study is mainly concerned with the parameters related to rock block. Therefore, for the sake of completeness of the discussion, it has been mentioned, but will be omitted in subsequent discussions of the remaining parameters to be compared.

From what has been analyzed so far, it can be seen that volume has a certain effect on all the parameters extracted from the Abaqus/CAE software simulation, so it is

a parameter that will not be neglected. This relationship will be confirmed by the machine learning algorithm subsequently implemented.

4.2.2 Traslational velocity

Acceleration

The impact acceleration of the block on the barrier depends on how the kinetic energy is dissipated by the net. The relation between the decelerating force of the block F and the acceleration of the block itself is already known:

$$F_d = ma$$

The impact force depends on the initial speed of the block (v), the stopping distance (Δs), and the response of the barrier. The energy of the block related to its movement will be:

$$E_k = \frac{1}{2}mv^2$$

This energy must be dissipated during impact, mainly in the form of barrier deformation, heat and vibration. If the block comes to a complete stop, the work done by the barrier (force stopping distance) is equal to the initial kinetic energy:

$$F_d\Delta s = \frac{1}{2}mv^2$$

Dividing by Δs :

$$F_d = \frac{\frac{1}{2}mv^2}{\Delta s}$$

From which, substituting the acceleration with the formula 4.2.1, it will be:

$$a = \frac{F_d}{m} = \frac{\frac{1}{2}v^2}{\Delta s}$$

This means that $v^2 \propto a$, and this is what the following graph shows:

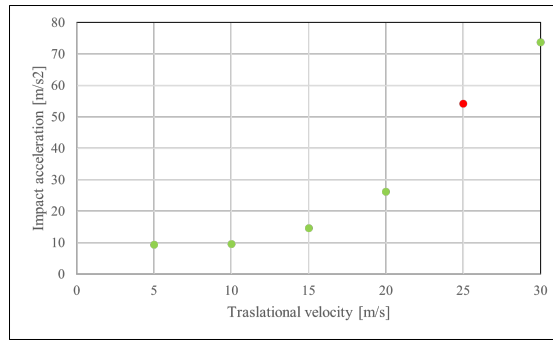


Figure 4.14: Relation between Impact acceleration and translational velocity of the block

Upper cable arrow

Always starting from the relation 5.1, this will be partly dissipated and partly absorbed by the barrier in the form of cable deformation. The work performed by the cable will therefore be:

$$W = E_{\text{absorbed}} = \frac{1}{2}mv^2$$

The work done by the cables is derived from the impact force and can be calculated as follows:

$$W = \int F dx$$

If we consider an elastic response of the net, it is possible to write:

$$F = k\Delta x$$

where:

- k is the cable elastic constant;
- Δx is the cable deformation.

Then substituting in 4.2.2 and solving the integral:

$$W = \frac{1}{2}k(\Delta x)^2$$

Balancing with the dissipated energy gives:

$$\frac{1}{2}mv^2 = \frac{1}{2}k(\Delta x)^2$$

Isolating displacement:

$$\Delta x = \sqrt{\frac{m}{k}} \cdot v$$

Thus it is clear that displacement is directly proportional to translational velocity ($v \propto \Delta x$), as it is confirmed by the following figure.

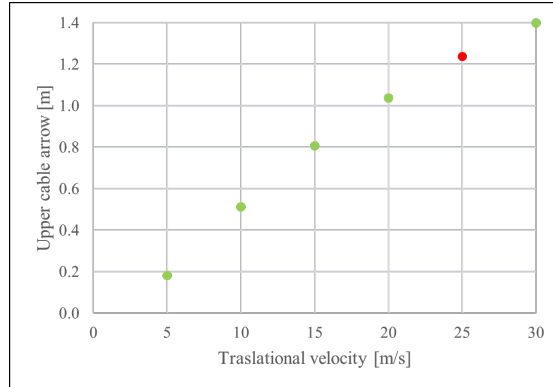


Figure 4.15: Relation between deformation of the upper cable and translational velocity of the block

The displacement is also influenced by the mass of the block and the stiffness of the cable:

- A stiffer cable offers more resistance, reducing deformation.
- A heavier block amplifies the deformation.

In practice, the effect of block speed on the network, briefly described here in terms of cable deformation, results in greater deformation the greater the speed. In order to reduce the effects of velocity, which are not adjustable at the level of the block, one can act on the number of cables in order to distribute the energy and reduce the effects of impact.

Kinetic energy

As already defined so far, the reference relationship is the previous 5.1, which we need to elaborate on by defining the energy variation between:

- E_{impact} ;
- E_{initial} ;

Following this scheme is it possible to write:

$$\Delta E = \frac{1}{2}m(v_{\text{impact}}^2 - v_{\text{initial}}^2)$$

From which the relationship $v^2 \propto \Delta E$, namely a parabolic relationship.

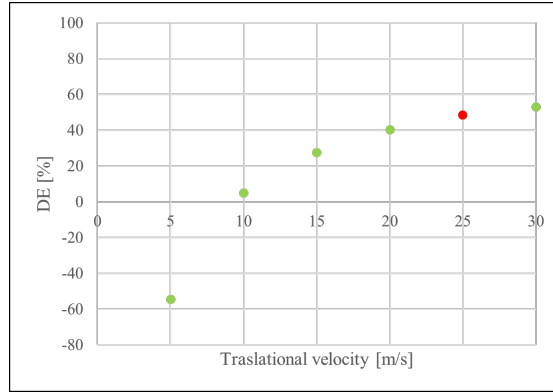


Figure 4.16: Relation between Energy variation during the impact and rotational velocity of the block

As with volume, speed is also of considerable importance, so this parameter will not be neglected but will be an integral part of the model realized.

4.2.3 Rotational velocity

Acceleration

The relationship between the acceleration of the block and its rotational velocity (ω) is related to the conservation of angular momentum and how the forces are distributed during impact. Given the initial speed of the block, its angular momentum will be:

$$L = I\omega$$

if I is the moment of inertia with respect to the rotational axis. During impact, the angular momentum may be partially transferred to the network or modified by external forces, which, however, are neglected due to simplification of the model sought. The angular velocity of the block could generate tangential reaction forces from the mesh, because the mesh contact point could generate a moment due to the rotation of the block. The angular velocity of the block could generate tangential reaction forces from the mesh, because the mesh contact point could generate a torque moment due to the rotation of the block. The resulting moment can be

calculated as:

$$\tau = rF_t$$

in which:

- r is the block radius;
- F_t is the tangential force.

It will influence angular velocity. As for the translational acceleration (a) of the block, it is related to the normal force (F_n) according to 4.2.2. This latter force can be related to the rotational velocity if there are interactions between the block and the mesh such as adhesion. Therefore, combining the effects of translational and rotational velocity, we obtain that:

$$a = \frac{F_n}{m} + \frac{\tau}{I} = \frac{F_n}{m} + \frac{\tau}{L\omega}$$

a high rotational speed (ω) can increase the tangential acceleration through (τ) provided there is adequate interaction with the network (e.g. friction or deformation).

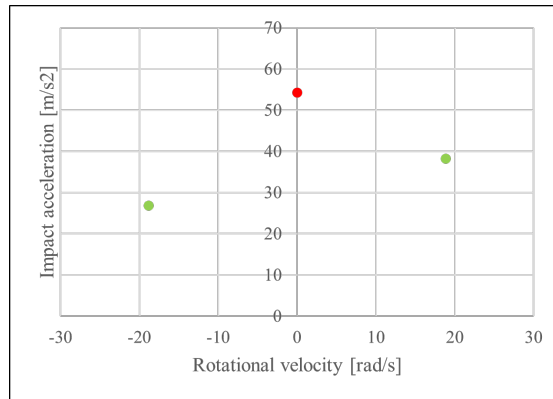


Figure 4.17: Relation between Impact acceleration and rotational velocity of the block

The fact that for a higher rotational velocity, the acceleration values decrease probably means that the interactions between the block and the mesh were not sufficient to establish the torque and therefore all previous considerations fell. However, it can be seen that the variations in the acceleration value do not appear to be exaggeratedly high, which will lead to the choice of neglecting this parameter.

Upper cable arrow

In this case, we no longer speak of translational energy, which was discussed in the previous subsections, but the rotational energy equal to:

$$E_{\text{rot}} = \frac{1}{2} I \omega^2$$

During impact, some of this energy can be transferred to the upper cable in the form of elastic deformation, if there is an effective interaction between the rotation of the block and the cable. The interaction between the block and the network manifests itself in the form of elastic deformation, which we can physically describe using Hooke's law:

$$\Delta y = \frac{F}{k}$$

considering that:

- F is the applied force to the cable;
- k is the elastic constant of the net
- Δy is the vertical deformation of the cable, directly proportional to the horizontal displacement.

This relation is valid considering an ideal composition of the cable, without dissipation. If F includes a tangential component induced by rotation, then:

$$\Delta y \propto r \omega$$

From which we derive a direct proportionality between cable deformation and angular velocity, as shown in the following graph.

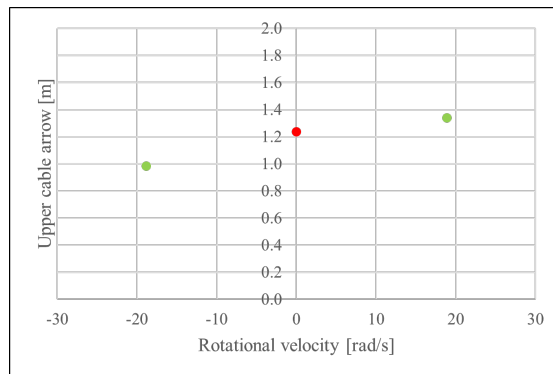


Figure 4.18: Relation between deformation of the upper cable and rotational velocity of the block

Kinetic energy

The change in total kinetic energy is related to the change in rotational velocity through the moment of inertia, as expressed in the relation 4.2.3, for which $E_{rot} \propto \omega^2$. The exact relationship, however, depends on the physical context (e.g. whether the motion is purely rotational or combined with translation).

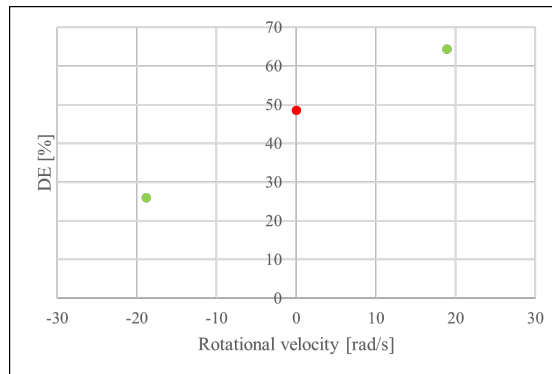


Figure 4.19: Relation between Energy variation during the impact and rotational velocity of the block

However, despite the theoretically identified relationships, there is little influence of the rotational component of the block velocity on the extrapolated parameters. For this reason it is excluded from the general discussion.

4.2.4 Impact angle

Acceleration

Observing the chosen reference system, one must emphasize the transition between the Cartesian system in which the valid components were v_x, v_y, v_z , and the reference system of the block moving with accelerated parabolic motion, for which a conversion from one system to the other is necessary, to obtain:

- Normal component $v_n = v \cos(\alpha)$;
- Tangential component $v_t = v \sin(\alpha)$.

The reference system is shown below:

At this point one can speak of normal speed and tangential speed with respect to the barrier, considering the angle of inclination with respect to the normal to the plane of the barrier as the angle of impact. The normal component of the force

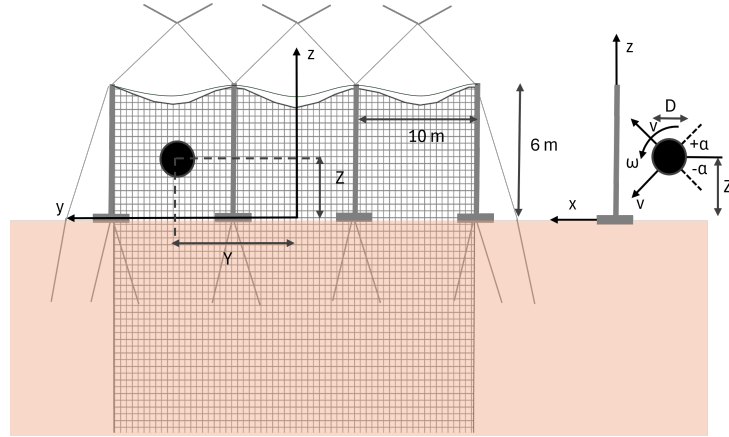


Figure 4.20: Structure diagram with reference system considered [Courtesy of Carriero MariaTeresa from her PhD thesis (in submission)]

is what causes the net to deform and slows down the blockage along v_n ; Deriving the acceleration by the velocity it is obvious that:

$$a_n \propto \frac{-v \cos(\alpha)}{\Delta t}$$

with Δt , time of impact.

The normal acceleration depends on the energy associated with it and the stiffness of the net, i.e. how quickly it can elastically dissipate the impact. Like the rotational speed, the tangential acceleration is also affected by possible friction with the network and local deformations that dissipate energy. The existing relationship is:

$$a_t \propto -\mu \sin(\alpha)$$

if μ is the friction coefficient with the net. The acceleration to be considered is the resultant of the two, i.e:

$$a = \sqrt{a_t^2 + a_n^2}$$

What is of interest for this study is the direct proportionality between α and acceleration, as is well demonstrated by the graph below.

The increasing trend depends on the predominance of the tangential acceleration, proportional to the sine of α , over the normal acceleration, proportional to the cosine of the angle, which would have led to a decrease in acceleration as the angle increased.

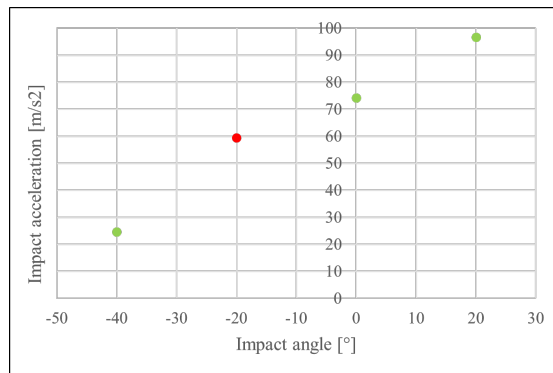


Figure 4.21: Relation between Impact acceleration and impact angle of the block

Upper cable arrow

To understand the relationship between the maximum displacement of the cable (f_{max}) and the angle of impact of the block on the net, it is essential to refer to the impact force. The latter can be divided into two components:

- Normal component $F_n = F \cos(\alpha)$
- Tangential component $F_t = F \sin(\alpha)$.

Considering the elastic behavior of the barrier, Hooke's law 4.2.3 is valid and allows to define proportionality $\Delta x \propto F$. In this case it is about normal component, as the impacts are predominantly perpendicular to the net, so it is expected a cosinoidal curve $\Delta x \propto \cos(\alpha)$.

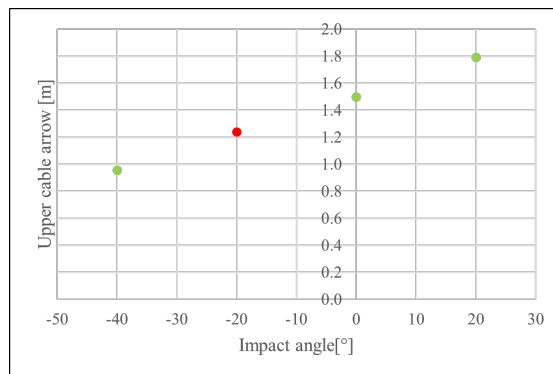


Figure 4.22: Relation between deformation of the upper cable and impact angle of the block

Kinetic energy

It is always necessary to decompose the normal and tangential components of the velocity, from which the normal and tangential energy component can be obtained. Taking up the speed decomposition already shown for the acceleration subparagraph (4.2.4), the resultant energy is:

$$E_k = E_k^n + E_k^t$$

where:

- $E_k^n = \frac{1}{2}mv_n^2 = \frac{1}{2}m(v \cos(\alpha))^2$
- $E_k^t = \frac{1}{2}mv_t^2 = \frac{1}{2}m(v \sin(\alpha))^2$

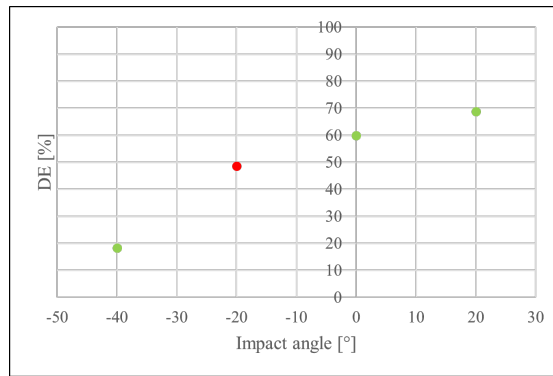


Figure 4.23: Relation between Energy variation during the impact and impact angle of the block

From the increasing sinusoidal graph we can see the prevalence of tangential energy $E_k^t \propto \sin^2 \alpha$.

4.2.5 Impact position along Y

The impact position (Y) directly influences:

- The distribution of forces on the network.
- The load that is transmitted to the upper and lateral posts.

Acceleration

The acceleration is directly related to force (see 4.2.2). The latter has a different influence considering the distance between the impact and the cables to which tension is generated.

- Impacts close to the supports generate greater tension in the cables due to less space for deformation.
- Impacts at the center of the barrier lead to greater global deformation, reducing the peak acceleration of the block.

In quantitative terms is true that: $a \propto F_{net}$, knowing that $F_{net} \sim \frac{1}{\Delta y}$.

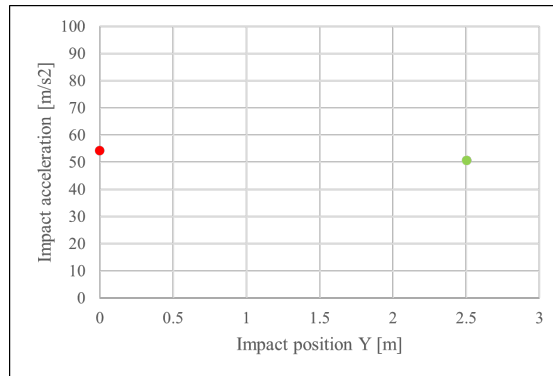


Figure 4.24: Relation between Impact acceleration and impact position along Y axis

Upper cable arrow

As the acceleration, even the cable deformation is influenced by the impact position:

- Impacts close to the supports generate a little deformation of the upper cable due to the dissipation along the supports.
- Impacts at the center of the net determine maximum since the cable must withstand a greater stretch to dissipate the energy of the block.

$$F_{net} \propto \frac{1}{\Delta y_{cable}}$$

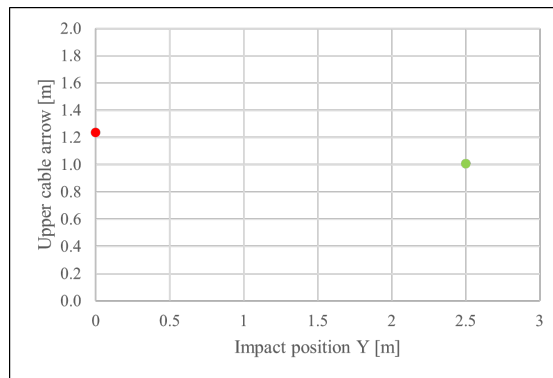


Figure 4.25: Relation between deformation of the upper cable and impact position along Y axis

Kinetic energy

As regard the kinetic energy:

- For lateral impacts the load is concentrated on the supports, with less overall dissipation;
- For central impacts, the mesh can better absorb the kinetic energy.

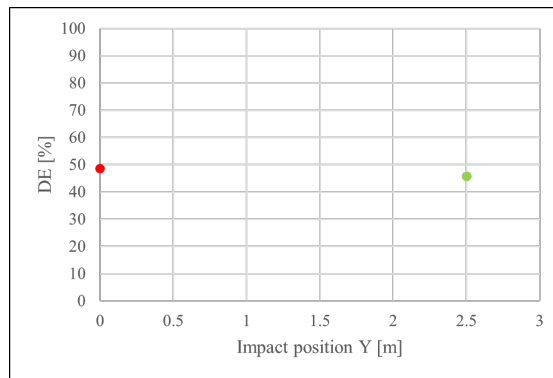


Figure 4.26: Relation between Energy variation during the impact and impact position along Y axis

However, despite the theoretically identified relationships, there is little influence of the impact position on the extrapolated parameters. For this reason it is neglected from the general discussion.

4.2.6 Impact position along Z

The impact position along the vertical axis can have an influence on:

- Upper cable if it is closer to it;
- Along the steel net, dissipating the energy above the whole interception net;

Acceleration

Block acceleration after the impact depends on the net reaction force, which varies according to the vertical position.

- Near the upper cable, the elasticity of the network is greater because the upper cable is less constrained than near the ground.
- Near the ground, it is possible that the block interact more with the slope, leading to lower acceleration.

The same relation of ΔY is still valid for ΔZ 4.2.5.

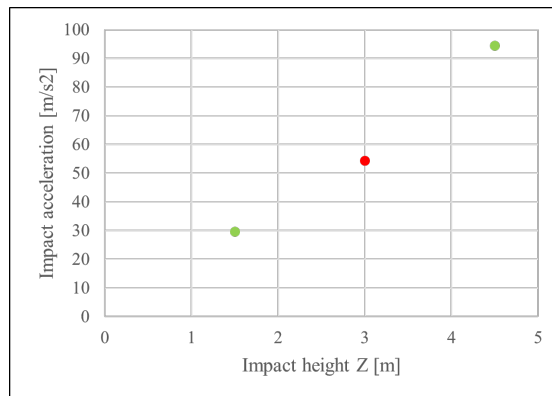


Figure 4.27: Relation between Impact acceleration and impact position along Z axis

Upper cable arrow

Logically, the deformation of the upper cable is directly proportional to the impact position along the vertical axis, $\Delta x \propto Z$. The closer the impact is to the upper cable, the greater its deformation. The further away it occurs, the less it will deform, thanks to the energy dissipation that has occurred along the lateral supports.

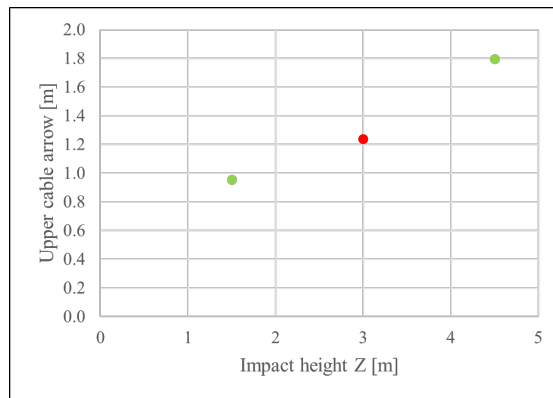


Figure 4.28: Relation between deformation of the upper cable and impact position along Z axis

Kinetic energy

The variation in energy in this case depends less on the impact position along the z axis, but rather is relative to the mode of dissipation that occurs. As already discussed:

- Near the upper cable, the rigidity of the net is higher, than the dissipation is higher.
- Near the ground, the block has more freedom of movement, so energy dissipation will be lower.

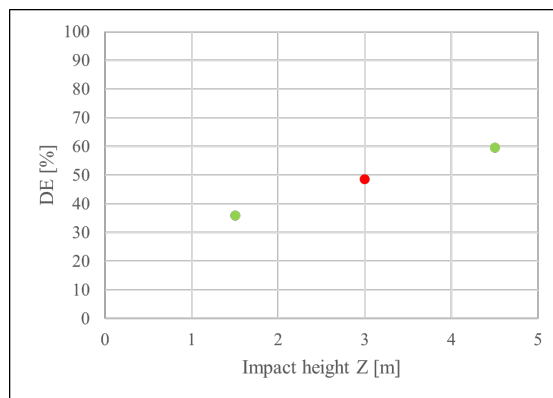


Figure 4.29: Relation between Energy variation during the impact and impact position along Z axis

Considering that the variation of the results is not negligible, this parameter is considered in the following analysis.

This sensitivity analysis was used to define the essential correlations between the parameters chosen in order to create a simplifying model for the design of the attenuator-type barrier, but also to initialize a machine learning algorithm which will be described in more detail in the following chapter and whose results will be set out, comparing them where possible with what emerged from the previous analysis.

From the analysis conducted, it emerged the importance of variables such as volume and translational speed in the design process of the interception system. In addition, an influence, albeit a minor one, was observed of the impact angle, which represents the direction of arrival of the block on the net, as well as the vertical position of the block itself. On the contrary, the rotational speed and the distance from the uprights of the block to the impact were found to have little influence, probably due to the panel width being insufficient to generate significant differences in the results. Consequently, it was decided to neglect these last two variables. A table summarising the choices made is presented below, in figure 4.30):

Input parameter	Influence	Range
Volume [m³]	yes	[0.02 – 2.4]
Traslational velocity [m/s]	yes	[5 – 25]
Rotational velocity [rad/s]	no	0
Impact angle [°]	yes	[-40 – +20]
Impact position Y [m]	no	0
Impact position Z [m]	yes	[1.5, 3.5, 4]

Figure 4.30: Influential parameters chosen for subsequent analysis

Chapter 5

Machine learning

Machine learning as we know it today originated with Arthur Samuel, an IBM researcher and pioneer of artificial intelligence, in 1959. However, its conceptual foundation dates back earlier, focusing on enabling computers to learn relationships between parameters without explicit programming [25]. Another key figure, Frank Rosenblatt, pioneered artificial neural networks with the development of the *perceptron*.



Figure 5.1: Machine learning applications [Bluewind]

Before getting to the heart of the realized model, a few words on the vast world of artificial intelligence to provide clarity.

Very often, there is confusion between artificial intelligence, machine learning and deep learning;

Artificial intelligence (AI)

AI represents a broad field of computer science that aims to endow machines with typically human capabilities, such as learning, reasoning and problem solving. The goal is to create systems capable of performing complex tasks autonomously, mimicking human intelligence.

Machine learning (ML)

Machine learning represents a subset of AI. It focuses on the ability of machines to learn from data. Through sophisticated algorithms, ML systems can analyze large amounts of data, identify patterns and relationships, and use this information to make decisions or perform tasks without being explicitly programmed. This capability is intended to be exploited in the present study in order to lay the foundations for more rapid future analysis for the complex design of rockfall barriers.

Artificial Neural networks (ANN)

They are positioned somewhere between ML and DL because they share functions with both, in some cases being absorbed into DL considering only their origin (inspired by the human mind) and their primary function: recognition of relationships for large amounts of data. Their characteristics will be explained in the following paragraph.

Deep learning (DL)

Deep learning represents a subset of ML. It is inspired by the workings of the human brain, is particularly suited to solving generalized problems requiring the understanding of large amounts of unstructured data: image recognition, natural language, text and image generation, etc.

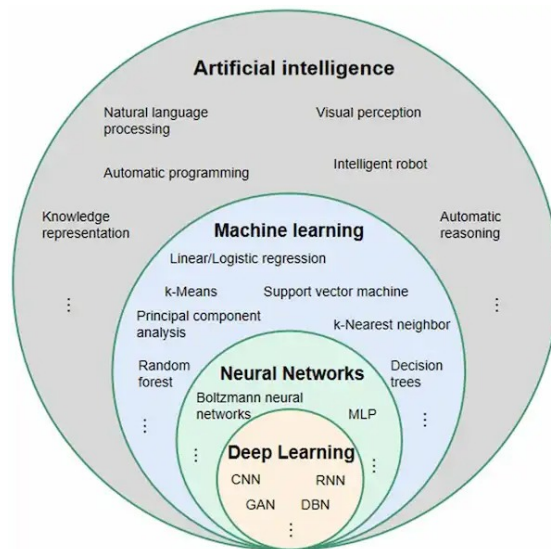


Figure 5.2: Relationship between AI, ML, Neural networks and DL [Machine Learning]

5.1 Machine learning

Machine learning (ML) can be categorized based on the training process into three main types: supervised learning, unsupervised learning, and reinforcement learning.

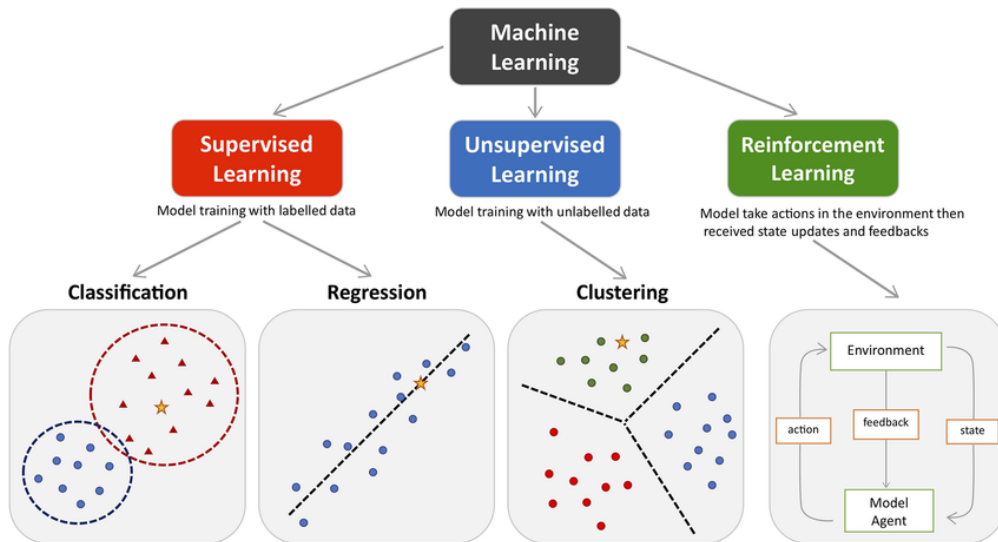


Figure 5.3: Different types of machine learning algorithm [25]

The main differences between these types of MLs are that:

- The supervised model is trained to recognize and trace data (inputs) to predefined classes (outputs). The data must be labeled for the training phase, as the outputs must be known a priori. The main algorithms used here are classification and regression.
- In the case of unsupervised learning, one does not have labeled data, but uses techniques such as clustering and associative analyses to model the data by creating homogeneous groups on the basis of their characteristics, based on concepts such as similarity or distance, even though the expected outputs are not known a priori.
- Reinforcement learning is particularly used in deep learning, it involves a series of sequential steps in which the analysis depends on both the characteristics of the data used for training and the current state of the system. These conditions allow the algorithm to make a prediction that will constitute the current state for the next cycle. Each cycle includes a reinforcement, a numerical reward signal, which is useful in encouraging the system to seek out the most favourable conditions. Otherwise, a penalty is applied.

This study examines the relationship between known input parameters (rock block impact conditions) and known output results (Abaqus/CAE simulations). Given that both input and output values are available, the study focused on **supervised learning** methods, specifically:

- Support Vector Machine (SVM)
- Artificial Neural Networks (ANN)

In collaboration with NTNU University, ANN was selected due to its capability to handle complex temporal predictions. The chosen approach involves **Long Short-Term Memory (LSTM)** networks to forecast system responses over time.

This chapter demonstrates how ANN can model the dynamic interaction between a rockfall and an interception system. By identifying hidden relationships in data, ANN facilitates the prediction of system behavior during impact. The process includes:

- Defining performance criteria
- Splitting and pre-processing data
- Selecting model inputs and architecture
- Training the network
- Validating the model

Ultimately, ANN is used to automate the extraction of impact-related parameters, eliminating the need for repeated individual simulations. These models can be used as a forecasting tool, complementing the process-based model and standard analyses such as those described in the previous chapter.

5.1.1 How it works - ML

The ML process involves several essential steps:

- **Data Collection**
 - Identifying relevant data sources
 - Evaluating dataset consistency for analysis
- **Data Preparation**
 - Data discovery and profiling

- Cleaning, transformation, and structuring
- Data enrichment for improved model performance
- **Model Training**
 - Selecting the appropriate algorithm
 - Processing training data to develop predictive models
- **Model Evaluation**
 - Testing accuracy with a validation dataset
 - Re-training if results fall below an acceptable threshold
- **Optimization and Tuning**
 - Enhancing accuracy while minimizing resource use
 - Techniques include feature engineering, hyperparameter tuning, and regularization
- **Implementation and Monitoring**
 - Deploying the model in real applications
 - Continuous monitoring to detect biases and update with new training data

By following this structured approach, the ANN model ensures robust, efficient, and scalable predictions for rockfall barrier impact analysis.

5.2 Artificial neural networks

Artificial neural networks (ANNs) are mathematical models designed to emulate the behavior of neurons in the human brain. They consist of interconnected nodes, called artificial neurons, which process and transmit information similarly to biological neurons.

The human brain is composed by more than 10 billion interconnected *neurons*: cells that uses biochemical reactions to receive, process and transmit information. Networks are formed by nerve fibres that create a sort of tree-like shape, called *dendrites*, connected to the *cell body* or *soma*, where the nucleus of the cell is located. From the *cell body* extends a single long fibre, called an *axon*, which eventually branches into filaments and subfilaments, and are connected to other neurons through synaptic terminals or *synapses*. The transmission of signals from one neuron to another at *synapses* is a complex chemical process, in which specific

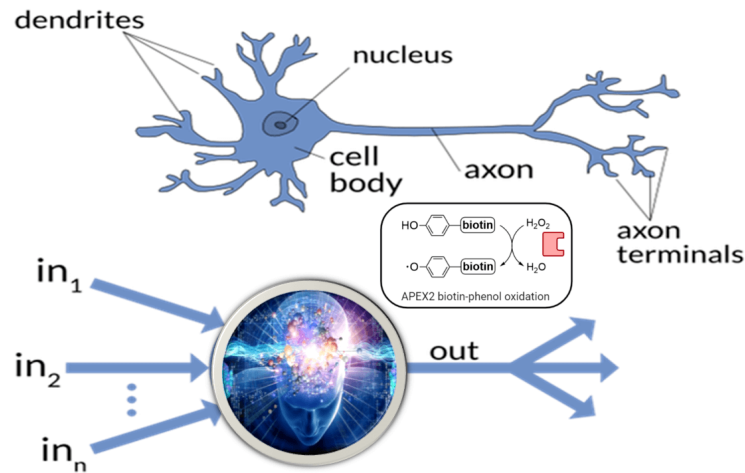


Figure 5.4: Similarity between neurons in the human body and neural networks [Dreams]

transmitter substances are released from the sending end of the junction. The effect is to raise or lower the electrical potential within the body of the receiving cell. If the potential reaches a threshold, an impulse is sent along the *axon* and the cell is ‘fired’ [26].

ANNs generalize these biological processes into artificial models where neurons receive inputs, process them using an *activation function*, and propagate outputs to subsequent layers. The activation function introduces non-linearity, allowing the network to learn complex patterns. This characteristic makes ANNs highly effective for tasks such as time-series forecasting, as demonstrated in applications like predicting the quantitative characteristics of water bodies [27]

5.2.1 How it works - ANN

The concept of artificial neurons was first introduced in 1943 [28]. The basic architecture consists of three types of neuron layers: input, hidden, and output layers [26]. The input layer takes input. The hidden layer processes the input. Finally, the output layer sends the calculated output [25].

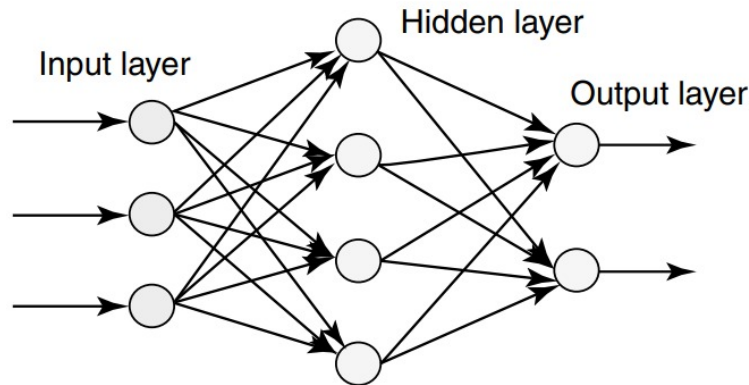


Figure 5.5: Multilayered artificial neural network [CNN]

Each connection between neurons has a weight that determines its importance. The learning process involves adjusting these weights based on training data using optimization techniques. Key functions in ANN training include:

Activation Functions

They determine whether a neuron should “fire” in response to an input. The most commonly used Functions are:

- *Sigmoid*: useful for outputs between 0 and 1.
- *ReLU (Rectified Linear Unit)*: widely used in deep networks because of its computational simplicity, which is why it was chosen in this discussion.
- *Softmax*: used for probability in multiclass classifications.

Optimization

The learning process involves optimization algorithms that minimize a loss function (loss function). Popular algorithms include *Stochastic Gradient Descent (SGD)* and variants such as *Adam*.

The latter has been used due to satisfactory results from the first implementation.

Regularization

To prevent overfitting, techniques such as *L1/L2 regularization*, *dropout* (random exclusion of neurons during training) or data augmentation (expansion of the dataset with variations in the data) are used.

Initially, regularization was underestimated, but improvements in results confirmed its importance.

Initialization of weights

Proper initialization is crucial to accelerate convergence and prevent problems like vanishing gradient. Techniques such as *Xavier Initialization* is commonly used.

Evaluation and Validation

Network performance is evaluated using appropriate metrics, such as accuracy. Techniques such as *cross-validation* are used to ensure that the model does not over-fit training data.

Once initialized, input data propagates through the network in a forward pass, generating an output. The error between predicted and actual results is then computed and back-propagated through the network to adjust weights, iterating over multiple epochs to refine predictions.

5.2.2 Feedforward vs. Recurrent Neural Networks

Feedforward networks allow information to flow only in one direction, making them effective for classification and regression tasks. However, sequential data requires a different approach.

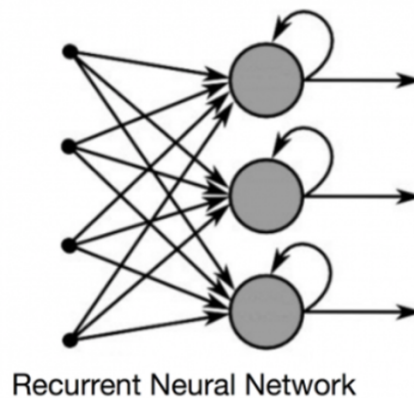


Figure 5.6: How recurrent neural network works [Deep learning]

Recurrent Neural Network introduce memory by maintaining connections across previous states. They process sequences like text and time-series data by incorporating prior inputs into current processing. Standard RNNs, however, suffer from the vanishing gradient problem, limiting their ability to capture long-term dependencies.

To address this, advanced architectures like *Long Short-Term Memory (LSTM)* and *Gated Recurrent Units (GRU)* were developed. LSTMs, used in this study,

efficiently capture temporal dependencies, making them ideal for modeling dynamic processes such as rockfall barrier impact analysis.

5.2.3 Benefits of ANNs

Traditional physics-based models are widely used to analyze complex systems, but they often require numerous parameters and extensive calibration, which can be time-consuming and may introduce inaccuracies due to necessary approximations.

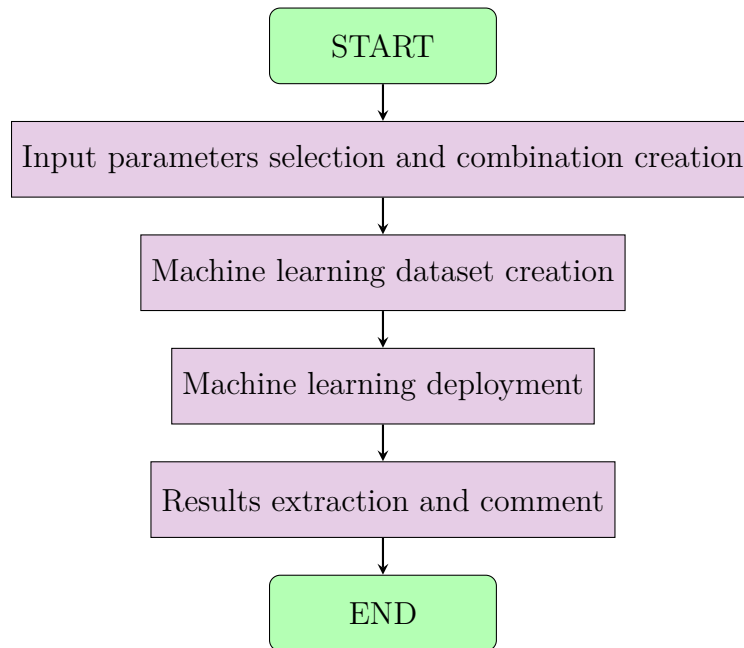
In contrast, data-driven methods like machine learning (ML) offer efficient alternatives by reducing dependency on predefined parameters and leveraging vast datasets for pattern recognition. Among ML techniques, ANNs stand out for their ability to model non-linear relationships and uncover hidden dependencies with high accuracy.

Despite their advantages, ANNs are not universally applied across all domains due to training complexity. However, once trained, an ANN simplifies into a computationally efficient algebraic model with fixed coefficients, enabling rapid predictions. This makes them particularly useful for iterative and real-time applications. Additionally, ANNs are highly adaptable, allowing integration with evolving system constraints and new data.

The increasing adoption of data-driven techniques highlights their value in modern engineering and scientific workflows. By efficiently handling complex datasets and minimizing dependency on predefined assumptions, ANNs provide scalable, dynamic, and highly accurate predictive modeling solutions [27].

5.3 Global sensitivity analysis

Below is a graphic diagram of the process followed for clarity of exposition; the individual steps will be detailed later.



5.3.1 Input Parameter Selection

As discussed in Chapter 4, the second sensitivity analysis was performed using Python scripts to implement a machine learning algorithm. The initial parameter definitions remained consistent across both analyses. However, while the previous approach examined variations in a single parameter at a time, this analysis utilized a Python script to generate all possible combinations of input parameters.

Notably, the number of input parameters was reduced from six to four. During the local analysis, it was observed that the impact position of the block on the panel's vertical axis and its rotational speed had minimal influence on the results. Consequently, these parameters were omitted. The setup configuration remains the same as described in Section 4.1.

The elasticity, panel length, and slope inclination parameters remained unchanged, as modifying them required manual adjustments in Abaqus. The model setup, as defined in Chapter 3, was adopted from [23].

Each set of input parameters was paired with Abaqus/CAE simulation. 576 sets were formed using Python but were removed due to the inclusion of invalid results. The errors were caused by Abaqus simulation errors that prevented the system from generating output correctly, while some variables never had values assigned to them. As there was such a large amount of valid data left, it was decided to disregard the invalid combinations and deal with the proper ones, rather than having to begin again from scratch in the software. The final dataset included 568 valid simulations, which provided sufficient data for machine learning implementation. The extracted

ID	V	v	ω	alfa	Y	Z
	[m ²]	[m/s]	[rad/s]	[°]	[m]	[m]
1	1.20	25	0	-20	0	3
2	0.09	25	0	-20	0	3
3	2.38	25	0	-20	0	3
Vol1	0.02	25	0	-20	0	3
Vol2	0.05	25	0	-20	0	3
Vol3	0.20	25	0	-20	0	3
Vol4	0.49	25	0	-20	0	3
Vol5	0.79	25	0	-20	0	3
4	1.20	10	0	-20	0	3
5	1.20	30	0	-20	0	3
Vel1	1.20	5	0	-20	0	3
Vel3	1.20	15	0	-20	0	3
Vel4	1.20	20	0	-20	0	3
8	1.20	25	0	20	0	3
9	1.20	25	0	0	0	3
10	1.20	25	0	-40	0	3
12	1.20	25	0	-20	0	1.5
13	1.20	25	0	-20	0	4.5

By combining all the input variables was derived 576 configurations

Trough the script *A_per creare combinazioni.py*

ID	V	v	ω	alfa	Y	Z
	[m ²]	[m/s]	[rad/s]	[°]	[m]	[m]
1	2.38	10	0	20	0	1.5
2	2.38	10	0	20	0	4.5
3	2.38	10	0	20	0	3
4	2.38	10	0	0	0	1.5
5	2.38	10	0	0	0	4.5
6	2.38	10	0	0	0	3
7	2.38	10	0	-40	0	1.5
8	2.38	10	0	-40	0	4.5
9	2.38	10	0	-40	0	3
10	2.38	10	0	-20	0	1.5
11	2.38	10	0	-20	0	4.5
12	2.38	10	0	-20	0	3
13	2.38	30	0	20	0	1.5
14	2.38	30	0	20	0	4.5
15	2.38	30	0	20	0	3
16	2.38	30	0	0	0	1.5
17	2.38	30	0	0	0	4.5
18	2.38	30	0	0	0	3
19	2.38	30	0	-40	0	1.5
20	2.38	30	0	-40	0	4.5
21	2.38	30	0	-40	0	3
22	2.38	30	0	-20	0	1.5
...

Figure 5.7: Input parameter combinations: local analysis (left) and global analysis (right).

results, stored in a dedicated folder, included:

- Block acceleration over time to determine the maximum deceleration (a_{max}).
- Displacement of the central point of the upper cable to determine the maximum deflection (f_{max}).
- Temporal evolution of block kinematic conditions ($a_x, a_y, a_z, v_x, v_y, v_z, u_x, u_y, u_z$).
- Energy variations, starting from the block's initial kinetic energy.
- Contact angle α , indicating the portion of the block in contact with the panel.
- Net stresses (though not the primary focus of this thesis).

This dataset provided a comprehensive basis for training the machine learning model, ensuring robust predictive capabilities.

5.3.2 Machine Learning Dataset Creation

Each parameter was stored in a dedicated file. Given that each combination generated thirty-five files, manual file processing was impractical. Python scripts were used to aggregate and structure the data into a single table.

To optimize the dataset, only the time interval from **0.00s** to **0.30s**—corresponding to the impact phase—was considered, reducing the original 5-second analysis window.

The input values, originally stored as text files, were combined with the output data into a single structured table, named "*merged output.xlsx*". Additionally,

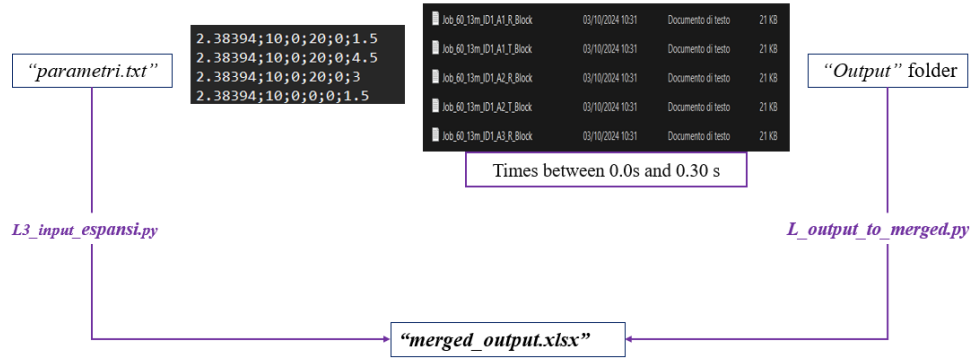


Figure 5.8: Python scripts used to create the machine learning dataset.

several key variables were computed using the Pythagorean sum of extracted components, as shown in the following Python code snippet:

```

1 expected_groups = {
2     "FRECCIA_MAX_CAVOSUP": ["U1_CAVOSUP", "U2_CAVOSUP", "U3_CAVOSUP"],
3     "A_T_Block": ["A1_T_Block", "A2_T_Block", "A3_T_Block"],
4     "V_T_Block": ["V1_T_Block", "V2_T_Block", "V3_T_Block"],
5     "V_R_Block": ["V1_R_Block", "V2_R_Block", "V3_R_Block"],
6     "RF_MDX": ["RF1_MDX", "RF2_MDX", "RF3_MDX"],
7     "RF_MSX": ["RF1_MSX", "RF2_MSX", "RF3_MSX"],
8     "RM_MDX": ["RM1_MDX", "RM2_MDX", "RM3_MDX"],
9     "RM_MSX": ["RM1_MSX", "RM2_MSX", "RM3_MSX"],
10 }

```

On the left, the names of the summed variables are listed, while the bracketed values represent their respective components. Both the individual components and the computed sums were included in the final dataset.

Computed Variables

Additional key values were computed as follows:

- **Translational Kinetic Energy**, computed as:

$$E_k = \frac{1}{2}mv^2 \quad (5.1)$$

- **Rotational Kinetic Energy**, computed as the difference between the total kinetic energy extracted from Abaqus/CAE ("*KE Block*") and the translational kinetic energy:

- **Block Acceleration**, computed as the derivative of translational velocity:

$$\mathbf{a}_{\text{tot}} = \left(\frac{dv_x}{dt}, \frac{dv_y}{dt}, \frac{dv_z}{dt} \right) \quad (5.2)$$

Final Dataset and Machine Learning Integration

The final dataset, structured as described above, was ready for machine learning implementation. All processing steps were executed through a single command in "*main.py*", which also included the execution of the LSTM algorithm, described in the next section.

5.3.3 Machine Learning Deployment

This problem involves multivariate forecasting with static input dependencies. Four constant input parameters act as additional features influencing the prediction of twenty time-dependent outputs. Given the complexity and sequential nature of the data, an LSTM (Long Short-Term Memory) model was chosen. LSTM networks effectively capture long-term dependencies, and constant inputs were concatenated as additional features during training. Regularization techniques, including dropout, were applied to enhance generalization due to the limited number of input combinations.

While the LSTM model learns time dependencies, it does not inherently compute statistical correlations. Therefore, correlation analysis was performed separately. Initially, correlations were calculated based on statistical measures such as mean, covariance, and standard deviation across entire columns. To refine this, correlations were also evaluated at the moment of impact (when a key variable reached its peak) and in adjacent time frames for greater precision. Both methods were implemented and later implemented.

The model processes the preformatted dataset row by row. In failure cases, the algorithm logs the issue and returns a "Failure" status. In successful cases, simulation data are stored and used for both correlation analysis and predictive modeling.

Correlation Matrix

Correlation analysis was conducted to compare relationships with local sensitivity analysis, monitor model performance, and serve as an additional validation metric. A key objective was to simplify rock block design by automating the search for parameter relationships, reducing reliance on manual analyses. The algorithm is trained to identify the maximum acceleration value of the block, calculated as a derivative of the velocity, and then extrapolate from the dataset the previous two

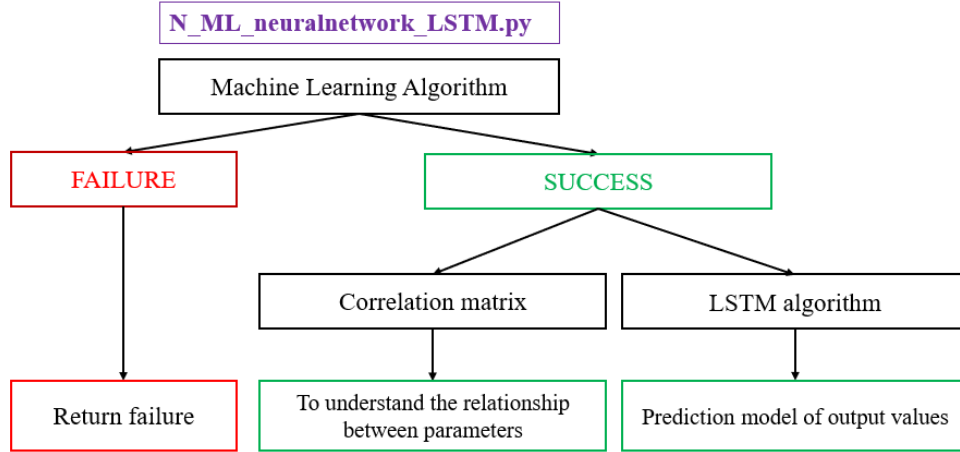


Figure 5.9: Flowchart of machine learning algorithm

rows and the next two rows and, for each combination, apply Pearson's correlation to these values. The Pearson correlation coefficient was computed using *pandas* (*DataFrame.corr()*) to quantify linear relationships between variables:

$$r = \frac{\sum_{i=1}^n (x_i - \bar{x})(y_i - \bar{y})}{\sqrt{\sum_{i=1}^n (x_i - \bar{x})^2} \sqrt{\sum_{i=1}^n (y_i - \bar{y})^2}} \quad (5.3)$$

where:

- x_i, y_i : observed values of variables x and y ;
- \bar{x}, \bar{y} : mean values of x and y .

A positive product $(x_i - \bar{x})(y_i - \bar{y})$ indicates that both variables tend to be above or below their mean simultaneously, while a negative product suggests an inverse relationship. The denominator normalizes covariance, yielding a correlation coefficient between -1 (strong negative correlation) and +1 (strong positive correlation), while values near zero indicating little or no correlation.

To visualize correlations, heat maps were generated using *seaborn* (*sns.heatmap*). Correlations were examined for the following groups:

- Input parameters;
- Output parameters carried out at impact time (velocity, acceleration, upper cable displacement, net forces, and moments);
- Output parameters after the impact (trajectory and energy dissipation).

This separation as a function of time is linked to the need to extrapolate the results as meaningful as possible; in fact, as far as velocity and acceleration are concerned, it is important to know their maximum value because this is what determines the deformation of the network. Whereas with regard to trajectory and energy, it is important to consider their final variation, i.e. how much energy is dissipated in the entire process.

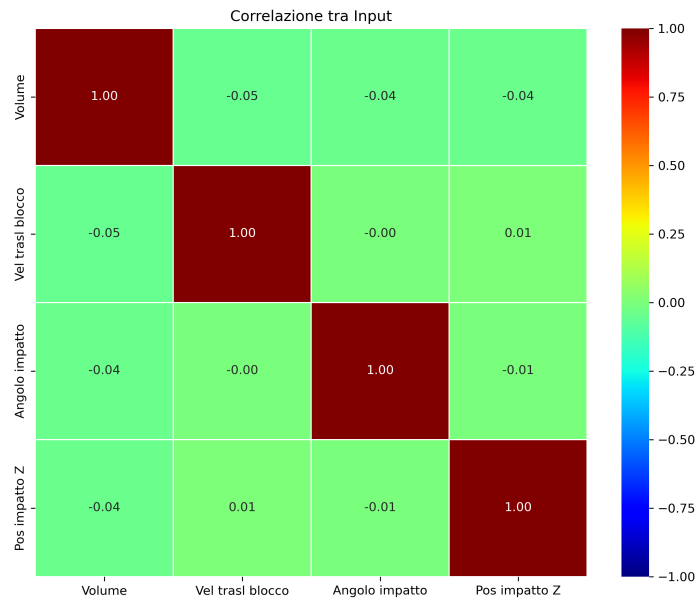


Figure 5.10: Correlation between input parameters.

As shown in Figure 5.10, input parameters are largely uncorrelated, with correlation values close to zero. Concerning non-parametric analyses, it is possible to define distributions of values without having to make assumptions about the shape of the distributions themselves. In particular, instead of assuming a specific model, one can proceed by analysing the correlation between the input parameters. In this approach, it is not necessary to make a priori assumptions about the nature of this correlation, but is sufficient to calculate its actual degree. Based on this calculation, the variables with the lowest correlation between them can be selected, thus reducing the risk of multicollinearity and improving the robustness of the analysis.

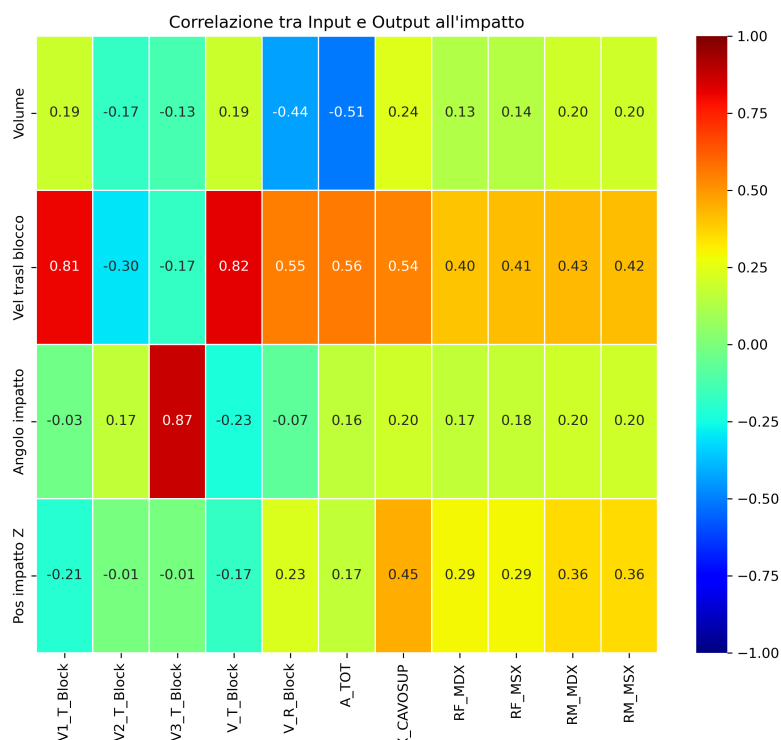


Figure 5.11: Correlation between input parameters and outputs at impact time

In the graph above, all the correlations between the values used as input and output values extrapolated at the impact time, set as 0.15 seconds were analyzed. In particular, it was identified the velocity where present 'V', the acceleration or rather, deceleration of the block 'A' and, finally, the barriers parameters. For each of these quantities, there are several terms; in the case of translational velocity, it was chosen to define both the Cartesian components individually and the resultant as it can give us a global indication of the intensity.

The values obtained confirm what was observed with the local sensitivity analysis, e.g. volume is inversely proportional to acceleration, as also shown in figure 4.27. As regards the maximum displacement of the upper cable of the interception system ("*freccia_{max-cavosup}*" in the correlation matrix 5.11), which gives an idea of the maximum elongation undergone by the net during impact. Fourth and third last columns refer to the reaction forces of the right and left posts respectively. The penultimate and last columns finally refer to the reaction torque when the uprights react to the impact of the block.

These results should be interpreted carefully and critically: they have been included for the sake of completeness but do not provide an exhaustive analysis. In fact, to

have a more detailed knowledge of what is happening to the net, the stress in the cables should be extracted, but this requires a more specific and in-depth study that can be implemented in the future.

What can be extracted from this matrix is that the velocity of the block and the impact position seem to have a greater influence than the other two variables involved, on the deformation of the upper cable; which is plausible because $v \propto \Delta x$, as exposed in figure 4.28. Similarly, the impact position plays a significant role; it is intuitive to consider that the closer the block impacts the cable, the greater the resulting deformation will be. In contrast, the impact angle appears to have only a minimal correlation with all observed variables. It can be said that this table best summarizes the core of the thesis whose aim was to know the relationships between the input values and the variation of the output parameters.

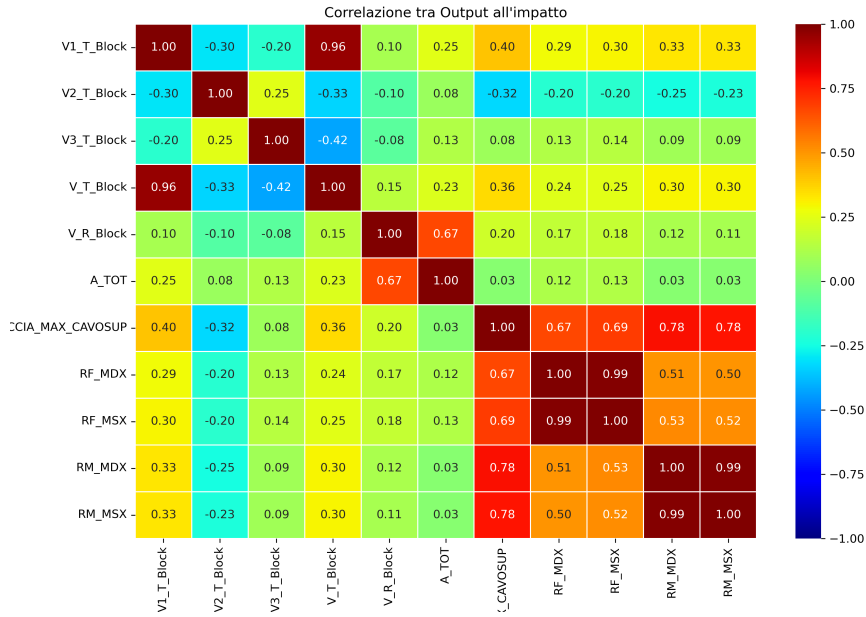


Figure 5.12: Correlation between output parameters at time of the impact

The graph presented in figure 5.12 simply represents how output values affect others, again extrapolated at the moment of impact. It is well known that the quantities referring to the interception system have a higher correlation with each other.

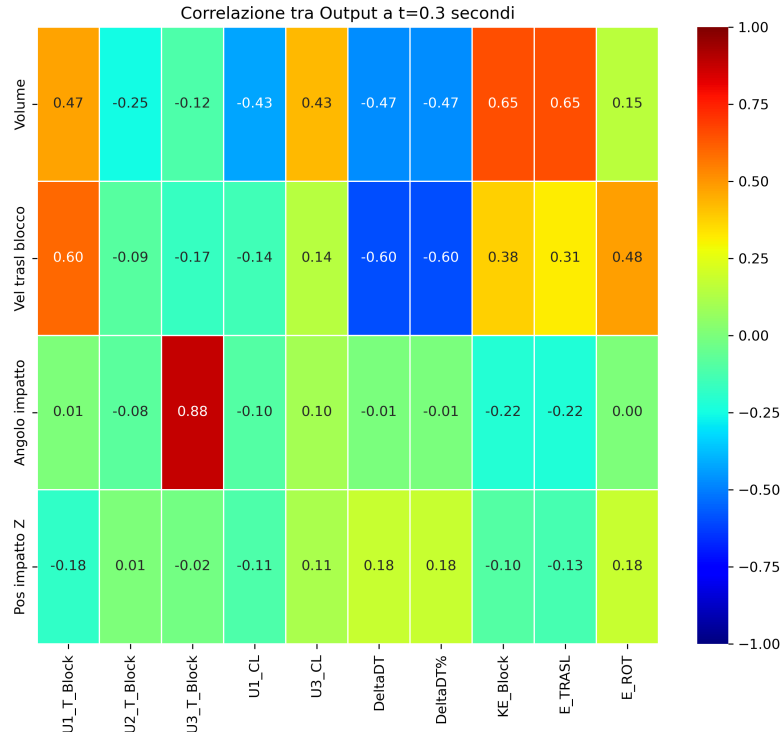


Figure 5.13: Correlation between inputs and outputs after impact time

Figure 5.13 presents the output values associated with the block, including its trajectory ($U1_T, U2_T, U3_T$) and total kinetic energy (KE_{Block}) which refers to the energy extrapolated from the Abaqus/CAE simulations, while the components ' E_{TRASL} ' and ' E_{ROT} ' were calculated during the preparation of the database as described in the previous section.

The trajectory of the block extracted from the software was compared to the components $U1, CL$ and $U3, CL$ which represent the trajectory that the block would have if it was not intercepted by the barrier. In particular, $U1$ indicates the trajectory along the x-axis, $U2$ along the y-axis transverse to the slope and finally $U3$ represents the vertical trajectory. We note the particular influence of the angle of impact on the trajectory along the vertical axis. This is related to the effect of gravity, which not only defines the speed, but also helps to establish the angle of incidence relative to the surface of the barrier. The variables that interest us most, however, are ' ΔDT ' and ' $\Delta DT\%$ ', which represent the difference between the free-fall trajectory and the trajectory with interception of the block by the

barrier, respectively, calculated as:

$$\Delta DT = U1_{T,block} - U1_{CL}$$

i.e. the trajectories with respect to the horizontal x-axis. And the relative percentage value given by ΔDT divided by $U1_{CL}$. The fact that there is a slightly marked negative correlation between the velocity and the trajectory suggests that as the velocity increases, the variation between the trajectories decreases, so there is less slowing down of the blockage by the barrier. These values are compared with the input variables.

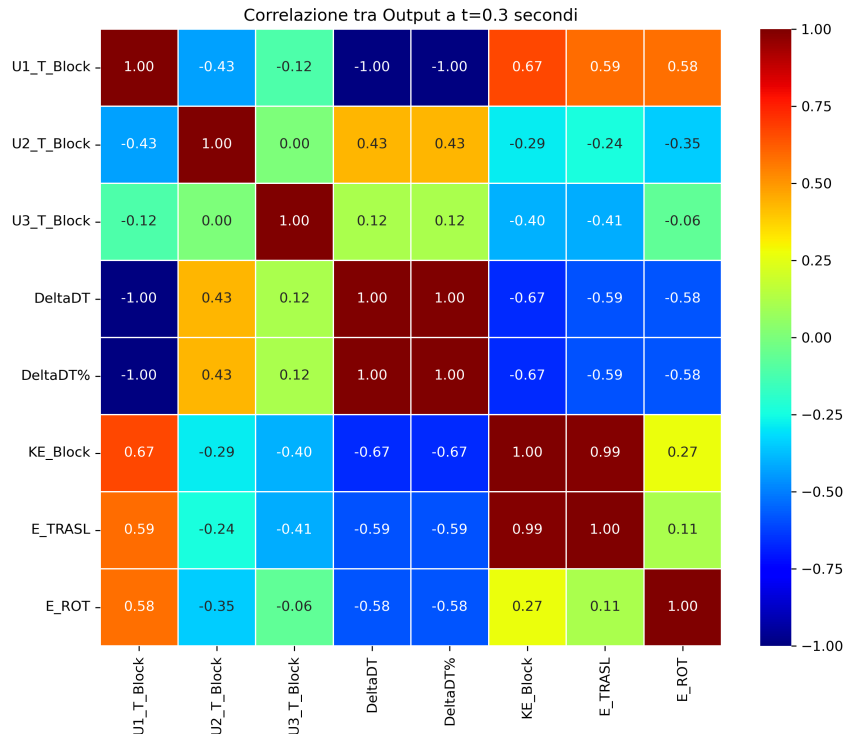


Figure 5.14: Correlation between outputs after impact time

As far as the influence that the output values have on the respective results is concerned, there is no particularly interesting evidence: it was already known that the difference between trajectories is certainly correlated with the trajectories themselves. What can be observed is rather the influence that the trajectory has on the energy variation. In particular, it can be seen that the trajectory along the x-axis is more correlated with the various forms of energy, unlike the others

trajectories. This leads one to think that as the trajectory increases, i.e. the further away the block arrives, the greater the energy associated with it, which is plausible. If an object is in motion, its kinetic energy is a function of its velocity, and if there is acceleration, its velocity is a function of the distance travelled. In this case we have an object subjected to a constant force, that of gravity and it is travelling along a trajectory: as its velocity increases as it moves, its kinetic energy (which is a function of velocity) increases.

It can be concluded that some parameters have a greater influence on others, so future analyses may take this as a starting point to focus on certain relationships rather than others. For example, the translational velocity and the angle of impact have importance with regard to the directionality of the block. A further key aspect concerns the confirmation of results from the local analysis. This implies that both analytical approaches possess validity and can be selected as reference methods for subsequent simulations.

Predictive model

The Long Short-Term Memory (LSTM) network is a type of recurrent neural network (RNN) that combines short-term memory with long-term memory through gating, which solves the problem of gradient disappearance [29].

This is possible introducing a memory cell and gating mechanisms that regulate the flow of information and determine which information to forget, retain, and output at each time step, enabling the network to capture both short-term and long-term dependencies.

At each time step, the LSTM operates as follows:

1. **Forget Gate:** The forget gate determines which parts of the previous cell state C_{t-1} should be forgotten. It takes the previous hidden state h_{t-1} and the current input x_t as inputs and applies a sigmoid activation:

$$f_t = \sigma(W_f[h_{t-1}, x_t] + b_f)$$

Here, $f_t \in [0,1]^d$ represents the forget gate's output, where d is the dimensionality of the cell state. Values close to 0 indicate forgetting, while values close to 1 indicate retaining.

2. **Input Gate:** The input gate decides which new information to add to the cell state. It has two components: a sigmoid layer that controls what to update and a tanh layer that generates candidate values:

$$i_t = \sigma(W_i \cdot [h_{t-1}, x_t] + b_i)$$

$$\tilde{C}_t = \tanh(W_C \cdot [h_{t-1}, x_t] + b_C)$$

Here, $i_t \in [0,1]^d$ represents the input gate, and $\tilde{C}_t \in [-1, 1]^d$ are the candidate values for the cell state.

3. **Cell State Update:** The cell state C_t is updated by combining the previous cell state C_{t-1} (scaled by the forget gate) with the candidate values \tilde{C}_t (scaled by the input gate):

$$\tilde{C}_t = \tanh(W_C \cdot [h_{t-1}, x_t] + b_C)$$

Here, \odot denotes element-wise multiplication.

4. **Output Gate:** The output gate determines the information to output from the current cell state as the hidden state h_t . It uses a *sigmoid activation* to control the output. The output gate equation is given by:

$$o_t = \sigma(W_o \cdot [h_{t-1}, x_t] + b_o)$$

And the hidden state update equation is:

$$h_t = o_t \odot \tanh(C_t)$$

In these equations:

- x_t : Input vector at time step t .
- h_{t-1} : Hidden state from the previous time step.
- f_t, i_t, o_t : Outputs of the forget, input, and output gates, respectively.
- C_t, C_{t-1} : Current and previous cell states, respectively.
- σ : Sigmoid activation function.
- \tanh : Hyperbolic tangent activation function.
- W_f, W_i, W_C, W_o : Weight matrices for the gates.
- b_f, b_i, b_C, b_o : Bias terms for the gates.

Model Architecture and Training Process

The LSTM-based predictive model is designed to include time dependencies and physical constraints in the training process. The model has the following key steps:

- *Data Initialization:* Providing values from extracted software reflecting the physical nature of the problem.

- *Data Pre-processing*: Normalization, missing data treatment, and train/test split.
- *Architecture Definition*: The architecture is composed of an LSTM layer to capture temporal relationships, followed by a fully connected (Dense) layer projecting latent features to output values. A ReLU activation function is employed, and dropout is included to avoid overfitting.
- *Model Training*: Weight optimization with backpropagation through time (BPTT) and Adam optimizer. Loss function is Mean Squared Error (MSELoss) with an additional physical loss term to ensure physical consistency. Model is trained for 50 epochs to minimize error on training and validation sets.
- *Validation and Testing*: Validation of the model's capacity to generalize to new data.
- *Prediction and Interpretation*: The training model predicts for dynamic inputs, scaling and normalizing back to their original scale for interpretation.

In order to judge the performance of the model, it is necessary to examine these stages and find out what is the most appropriate stage to include physical relationships. The total kinetic energy, quantified as the sum of its translational and rotational parts, and the two parts separately, has been incorporated at two different stages, and their impacts on model performance will be examined. For the sake of clarity, the speed trend over time is shown, comparing the values extrapolated by the software and the values simulated by the trained model. First of all, it is shown its trend referred to the physical model in figure 5.15:

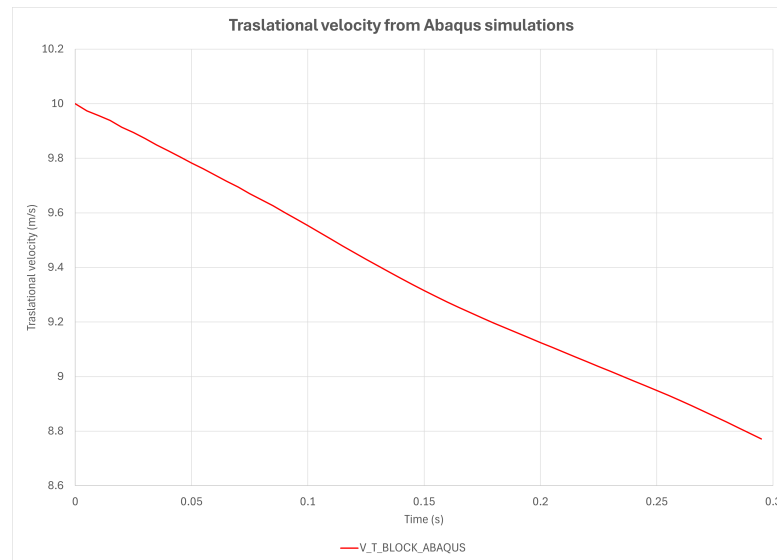


Figure 5.15: Traslational velocity extrapolated by Abaqus simulation

From this image, one should note the trend of the translational velocity - taken as an example to show the potential and criticality of the implemented model - which appears to be linear, decreasing as assumed due to the presence of the barrier that contributed to this reduction.

To compare the results of the model with simulations, three separate approaches were developed, each with specific peculiarities. Each model was tested on one or more iterations in order to assess the effect of training on the quality of the predictions.

Modification of the Training Function In the first trial, an additional polynomial regression was initially introduced during training, to allow the model to learn not only the numerical values, but also their time course, variable by variable. The physical relationships were incorporated in the data pre-processing phase, ensuring that they were already known during training.

The model was first trained for a single epoch (trend shown in blue) and subsequently for 25 epochs (trend in dark green, see figure 5.16).

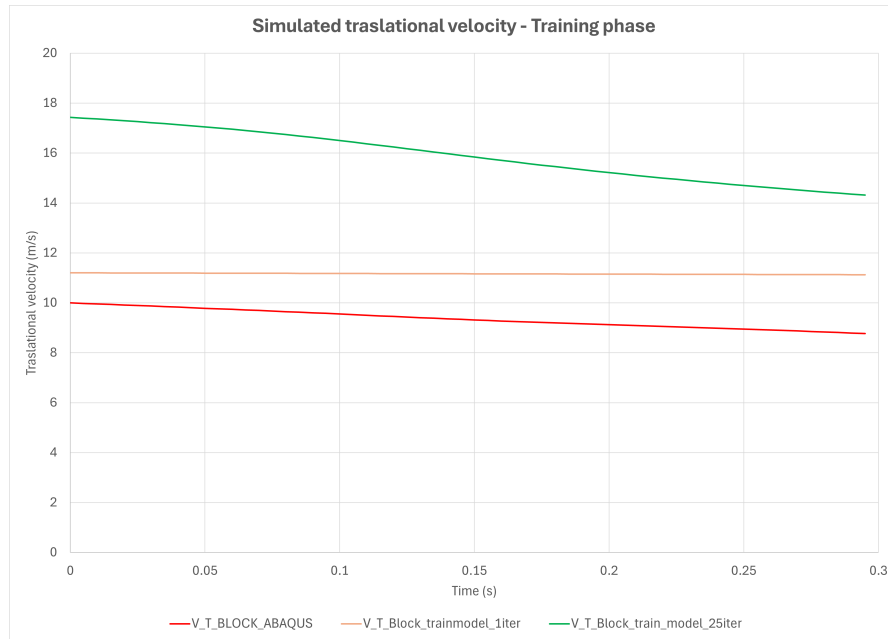


Figure 5.16: Velocity trend considering polynomial regression

The analysis of the results shows that, compared to the simulated data, the speed is initially overestimated after only one iteration, with a more stable trend, not visible decreasing. With more iterations, the trend remains similar to the physical one, but an greater overestimation of the values is observed. To improve accuracy, it would be necessary to introduce a relationship between the translational velocity provided as input and that extracted from the simulation.

Modification of Training function - Velocity only After 25 epochs, the loss function showed an increasing tendency, indicating that prolonging training was not beneficial. To improve learning, it was decided to reduce the dataset to the velocity and trajectory components only, from which acceleration and energy information could be derived.

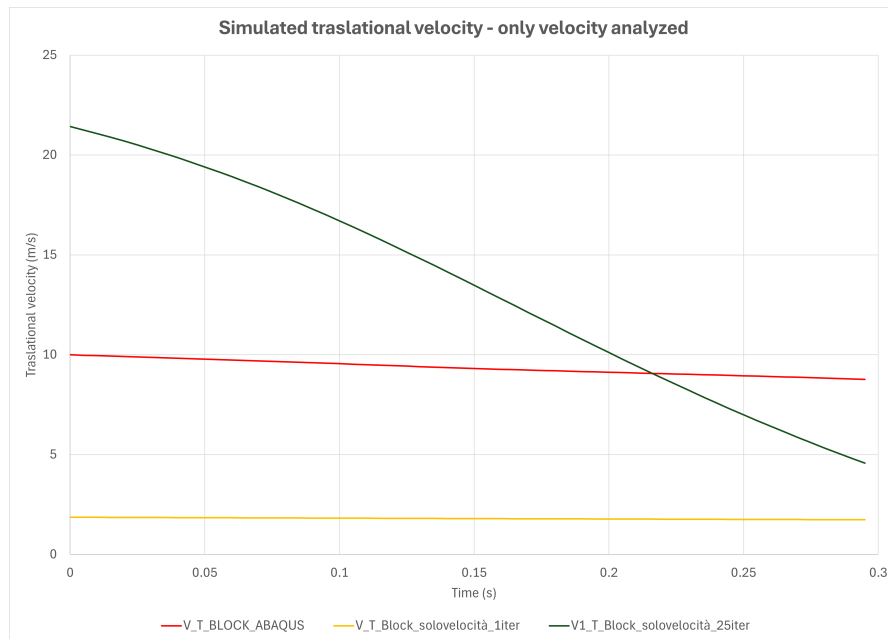


Figure 5.17: Velocity trend training the model only on speed values

Again, after only one iteration, the simulated velocity is underestimated (see light orange line in 5.17), but maintains time course more similar to the expected one. However, by increasing the number of iterations, both numerical consistency and the correct trend are lost, as seen through the green line in the above figure. This analysis suggests that the exclusive use of polynomial regression in the training phase is not sufficient for the model to correctly learn the physical relationships between variables over time.

Modification of simulation phase In light of the previous results, a different strategy was tried: letting the model train on the data from the dataset without additional constraints, and then correcting the simulated values in the post-processing phase by integrating the physical information of the problem.

It was observed that although the model manages to capture some implicit relationships between variables, it loses key information in the long run. For this reason, a regression-based correction of the simulated data was introduced.

- Without physical correction:

	Simulated velocity (V_T_Block)	
	batch size = 32	batch size = 64
1 Iteration	V_T_Block_1iter_nn_32	V_T_Block_1iter_nn_64
25 Iterations	V_T_Block_25iter_nn_32	V_T_Block_25iter_nn_64
100 Iterations	V_T_Block_100iter_nn_32	---

Figure 5.18: Combinations of simulated velocity extrapolated

- With physical corrections ("CALC" that means "calculated"):

	Calculated velocity (V_T_Block_CALC)	
	batch size = 32	batch size = 64
1 Iteration	V_T_Block_CALC_1iter_nn_32	V_T_Block_CALC_1iter_64bs
25 Iterations	V_T_Block_CALC_25iter_nn_32	V_T_Block_CALC_25iter_nn_64b
100 Iterations	V_T_Block_CALC_100iter_nn_32	---

Figure 5.19: Combinations of calculated velocity extrapolated

Starting from the analysis of the simulated velocity values (listed in figure 5.18), i.e. following the same procedure as in the two previous cases, we obtain the results presented in figure 5.20:

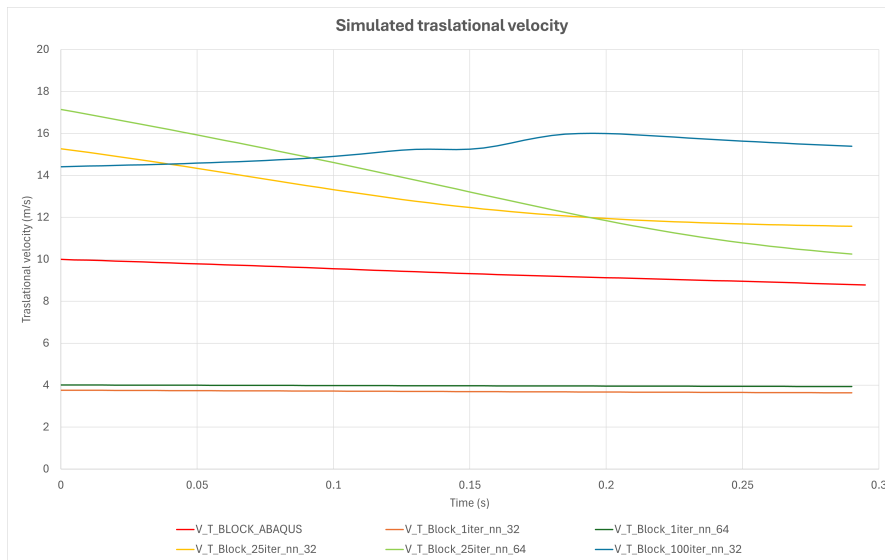


Figure 5.20: Simulated velocity without physical correction

Starting from the bottom in figure 5.20, the simulated velocity values corresponding to different batch sizes are depicted in orange and green for batch sizes of 32 and 64, respectively, after a single iteration. It is evident that in both cases, the velocity is significantly underestimated.

Upon increasing the number of epochs to twenty-five, the predicted curves exceed the target red reference curve. Moreover, a slight divergence is observed between the predictions for batch size 32 (yellow line) and 64 (light green line), with neither case accurately capturing the linear trend of the physical simulation.

Given the theoretical expectation that increasing the number of iterations should enhance the model's ability to capture latent relationships, the number of epochs was further increased to one hundred, maintaining a batch size of 32. However, the results were unsatisfactory, as both the numerical accuracy and the underlying trend of the system were lost.

Since these outcomes remained inconsistent with the desired behavior, a post-simulation correction was introduced by incorporating physical constraints. Specifically, the model was explicitly informed of the relationship between the translational velocity of the dynamically inserted block (used as input), while the energy and acceleration formulations—computed as the derivative of velocity—were iteratively updated.

The resulting predictions, incorporating these physical constraints, are presented in figure 5.21:

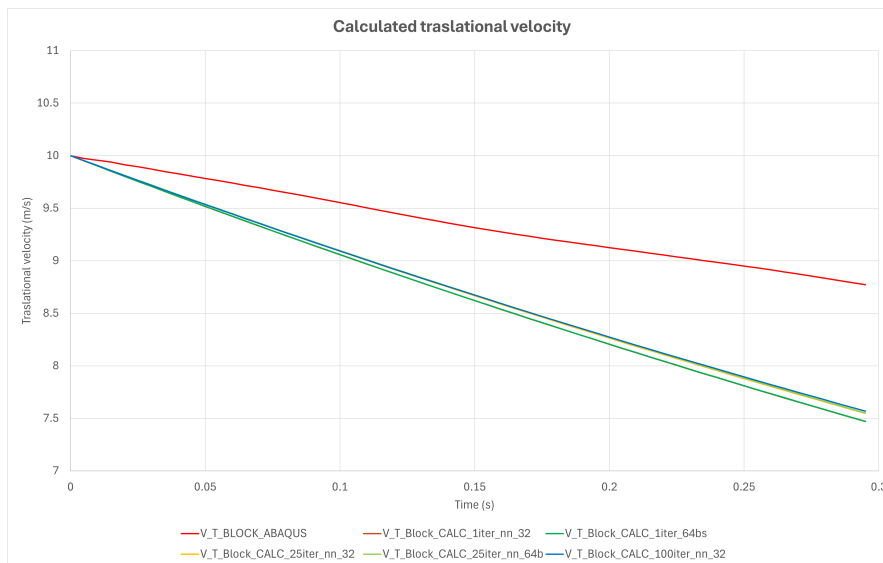


Figure 5.21: Calculated velocity without physical correction

From here it is much quicker to observe that the values are more consistent with the physical simulation to be obtained. The line that most underestimates the

velocity value, as in the previous cases, is the one derived from the simulation with a single iteration. For the remaining ones, there is not much difference between the various configurations, but the values all stabilize around 7.5 m/s. This suggests that the physical correction influences the simulation more, although the simulation from which the result is derived must also play a role. This approach ensured greater stability in the results. Although graphs of all the quantities analyzed are not shown to avoid excessive complexity, the observed behaviour for speed is also representative of the other variables.

In conclusion, it can be seen that in none of the different combinations is a perfect match with the velocity trend derived from Abaqus. The closest possibility is the addition of post-simulation physical relationships that force the model to be compatible with the reference physical trend.

The application of **machine learning (ML)** in geotechnical engineering for the design of rockfall barriers has demonstrated significant potential in enhancing predictive capabilities and optimizing structural performance. A key contribution of this study is the **construction of correlation matrices**, which not only provide insight into the relationships between existing parameters but also serve as a foundation for the integration of additional parameters in future analyses.

Furthermore, the implementation of a **predictive model** based on Long Short-Term Memory (LSTM) networks allowed for the simulation of system behavior. However, the results indicate that the trained model did not achieve a precise correspondence between the numerical simulations conducted in Abaqus and the ML-based predictions. This highlights the complexity of capturing highly nonlinear interactions in geotechnical systems solely through data-driven approaches, emphasizing the need for further refinement and the possible integration of additional physical constraints to improve model reliability.

All Python codes used in this thesis are collected in the following QR code (5.22).



Figure 5.22: QR code redirecting to the code's folder [link: GitHub]

Chapter 6

Epilogue

6.1 Conclusion

Attenuators play a primary role in risk reduction and safeguarding of infrastructure and natural scenery in rockfall barrier design. They reduce the energy of rock falls and lower their impact force, safely redirecting them to designated locations. One challenge is the lack of comprehensive and specific legislation, as standardized laws are required to ensure their optimal performance under different geological and environmental conditions. This gap highlight the necessity of conducting targeted analyses and developing advanced design methodologies to enhance the safety, efficacy, and versatility of rockfall attenuators. To conclude this thesis, we can highlight some key points regarding the three main areas of development: local sensitivity analysis, global sensitivity analysis and the implementation of the predictive model.

First, the local sensitivity analysis helped identify the most influential parameters in the design of rockfall barriers, such as the volume and speed of the block. Understanding these details is crucial optimizing barriers design so that they can more effectively counter diverse impact scenarios.

Global analysis, on the other hand, captured the complex interplay between variables, offering a broader view of the phenomenon.

Secondly, the application of a machine learning model demonstrated the potential capacity of the technology to support engineering development. Although the data is promising, further development is needed to refine the approximation of parameter relationships and improve the accuracy of prediction models. This work, however, is the first significant step toward integrating advanced techniques into infrastructure design and safety engineering.

The results obtained contribute filling a gap in the literature and provide concrete insights for practical application, proposing new tools to improve land

protection against rockfall risk. At the same time, the work paves the way for future developments, including the optimization of forecasting models, the expansion of the reference database and the integration of new artificial intelligence techniques to further refine the analyses.

In conclusion, this research not only addresses the topic from a theoretical perspective, but also from a real-world application standpoint, providing a foundation for the design of increasingly safe and high-performance protection systems.

6.2 Suggestion

The task undertaken in this research considered the parameters that, according to current legislation as well as literature reviews, are critical for rockfall barrier design. Nevertheless, the realized model can be seen as a starting point, meaning that there is potential for additional parameters be included and tested in the future. For example, beside the mass and velocity of the rock, variables on the retaining net might be considered in terms of its characteristics, such as its strength and capacity for energy dissipation. It would also be useful to consider other variables, such as the terrain type and topography of the area, which could significantly affect the effectiveness of the barriers. One other possible development concerns the coupling of parameters associated with the trigger causes of the phenomenon, e.g., seismicity or severe weather, that could modulate the boulder's behavior and response to the barriers.

One highly relevant following development could be creating more advanced predictive models, considering dynamic events such as the translation of blocks in several phases, instead of only impact moment.

As regards the machine learning-based predictive model, there is a requirement to keep it even more sophisticated. One of the ways it could be enhanced is by going deeper into the computer method so that the model can more accurately find correlations among parameters. To start with, it would be beneficial to train the model with fewer data and parameters, so as not to risk overfitting and to test it on a large dataset, but it is important knowing which parameters, this thesis will be helpful. Subsequently, only after the model has been shown to be stable, it will be feasible to implement it with more parameters and to optimize the predictions for various contexts. Finally, another suggestion for future work would be to include a physical simulation module, in order to compare the outcome of the model with actual simulations under some circumstances, making it even more credible.

It might also be beneficial to collect experimental data in the field, in order to make the model's predictions even more robust and increase its applicability.

Bibliography

- [1] *Rockfall Protection Kits*. 2018 (cit. on pp. 2, 19, 20).
- [2] Ali Mutar Fanos, Biswajeet Pradhan, Shattri Mansor, Zainuddin Md Yusoff, and Ahmad Fikri bin Abdullah. «A hybrid model using machine learning methods and GIS for potential rockfall source identification from airborne laser scanning data». In: *Landslides* 15 (2018), pp. 1833–1850 (cit. on p. 2).
- [3] Varnes and David J. «Landslide types and processes». In: *Landslides and engineering practice* 24 (1958), pp. 20–47 (cit. on p. 5).
- [4] D.M. Cruden and D.J. Varnes. «Landslide Types and Processes». In: *Special Report - National Research Council- Transportation Research Board* 247 (Jan. 1996), pp. 36–57 (cit. on pp. 6, 7).
- [5] G. Herrera et al. «Landslide databases in the Geological Surveys of Europe». In: *Landslides* (Oct. 2017). DOI: 10.1007/s10346-017-0902-z (cit. on p. 6).
- [6] <https://www.isprambiente.gov.it/it/progetti/cartella-progetti-in-corso/suolo-e-territorio-1/iffi-inventario-dei-fenomeni-franosi-in-italia> (cit. on p. 6).
- [7] *Dissesto idrogeologico in Italia: pericolosità e indicatori di rischio* (cit. on pp. 6–8).
- [8] Varnes D.J. «Landslide hazard zonation: a review of principles and practice.» In: *Commission on Landslides of the IAEG, UNESCO, Natural Hazards* (1984) (cit. on p. 8).
- [9] S.D. Pardeshi, S.E. Autade, and S.S. Pardeshi. «Landslide hazard assessment: recent trends and techniques». In: *SpringerPlus* 2 (2013) (cit. on p. 8).
- [10] «Rockfall characterisation and structural protection – a review». In: *Nat. Hazards Earth Syst. A.* (2011) (cit. on p. 9).
- [11] Hungr et al. «The Varnes classification of landslide types an update». In: *Research gate* (2014) (cit. on p. 9).
- [12] F. Vagnon, J.P. Harrison, A. M. Ferrero, and G. Umili. «Reliability based design for rock fall barriers». In: () (cit. on p. 10).

- [13] F. Bourrier, S. Lambert, and J. Baroth. «A Reliability-Based Approach for the Design of Rockfall Protection Fences». In: *Springer-Verlag Wien* (2014) (cit. on p. 11).
- [14] M. Cerro, G. Giacchetti, M. Lelli, A. Grimod, and A. Arul. «Hybrid rockfall barrier — new design methodology based on the Colorado full-scale test experience». In: *Australian Centre for Geomechanics, Perth, ISBN 978-0-9924810-5-6* (2016) (cit. on pp. 11, 12, 14, 19).
- [15] *Rockfall* (cit. on p. 18).
- [16] B. Arndt, T. Ortiz, and Turner. «Colorado’s full-scale field testing of rockfall attenuator systems». In: *Transportation Research Circular E-C141, prepared for the Transportation Research Board, sponsored by the Colorado Department of Transportation (CDOT)*. (2009) (cit. on p. 19).
- [17] A. Volkwein, W. Gerber, J. Klette, and G. Spescha. «Review of Approval of Flexible Rockfall Protection Systems According to ETAG 027.» In: *R Geosciences* (2019) (cit. on p. 20).
- [18] CEN members. *Eurocode 7: Geotechnical design*. Tech. rep. European Commission, 2004 (cit. on p. 20).
- [19] M. Marchelli, D. Peila, and V. De Biagi. «Reliability-Based Design of Protection Net Fences: Influence of Rockfall Uncertainties through a Statistical Analysis». In: (July 2020) (cit. on p. 21).
- [20] M. Marchelli, D. Peila, and V. De Biagi. «Reliability analysis and partial safety factors approach for rockfall protection structures». In: *Engineering Structures* (2020) (cit. on pp. 21, 22).
- [21] D. Toe, A. Mentani, L. Govoni, and al. «Introducing Meta-models for a More Efficient Hazard Mitigation Strategy with Rockfall Protection Barriers». In: *Rock Mech Rock Eng 51, 1097–1109* (2018) (cit. on p. 21).
- [22] F. Vagnon, S. Bonetto, A.M. Ferrero, J.P. Harrison, and G. Umili. «Eurocode 7 and Rock Engineering Design: The Case of Rockfall Protection Barriers». In: *geosciences* (2020) (cit. on p. 22).
- [23] M. T. Carriero, M. Migliazza, F. Vagnon, A. M. Ferrero, M. Nadalini, and L. Gobbin. «Towards reliability-based design of rockfall hybrid barriers and attenuators: A focus on the resistances». In: *Intervento presentato al convegno Proceedings of the ISRM European Rock Mechanics Symposium, EUROCK 2024 tenutosi a Alicante (Spain)* (15th -19th July, 2024) (cit. on pp. 24, 27, 30, 62).
- [24] J. P. Escallón, C. Wendeler, and M. Mrozik. «Numerical Simulation of the Impact of a Rock Fall Impact on a Flexible Barrier using Abaqus/Explicit 6.12». In: *All Days* (Oct. 2013) (cit. on p. 26).

- [25] Batta Mahesh. «Machine learning algorithms-a review». In: *International Journal of Science and Research (IJSR).[Internet]* 9.1 (2020), pp. 381–386 (cit. on pp. 53, 55, 58).
- [26] Ajith Abraham. «Artificial neural networks». In: *Handbook of measuring system design* (2005) (cit. on p. 58).
- [27] «An ANN application for water quality forecasting». In: *Marine Pollution Bulletin* 56.9 (2008), pp. 1586–1597. issn: 0025-326X (cit. on pp. 58, 61).
- [28] W.S. McCulloch and W. Pitts. «A logical calculus of the ideas immanent in nervous activity». In: *Bulletin of Mathematical Biophysics* 5, pages 115-223 (1943) (cit. on p. 58).
- [29] «Forecasting monthly gas field production based on the CNN-LSTM model». In: *Energy* 260 (2022), p. 124889 (cit. on p. 72).